

A PRELIMINARY ABUNDANCE ANALYSIS AND  
MICROTURBULENCE DETERMINATION  
FOR THE PECULIAR A-STAR  
BETA CORONAE BOREALIS

BY

RONALD MARCUS OPITZ

Bachelor of Science

East Central Oklahoma State University

Ada, Oklahoma


1971

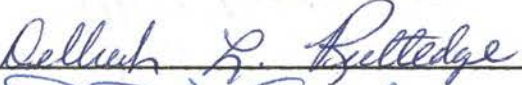
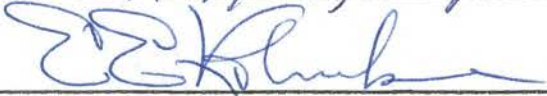
Submitted to the Faculty of the Graduate College  
of the Oklahoma State University  
in partial fulfillment of the requirements  
for the Degree of  
MASTER OF SCIENCE  
December, 1974


MAR 28 1975

A PRELIMINARY ABUNDANCE ANALYSIS AND  
MICROTURBULENCE DETERMINATION  
FOR THE PECULIAR A-STAR  
BETA CORONAE BOREALIS

Thesis Approved:

  
\_\_\_\_\_  
Thesis Adviser

  
\_\_\_\_\_  
  
\_\_\_\_\_

  
\_\_\_\_\_  
Dean of the Graduate College

903423

## ACKNOWLEDGEMENTS

The author wishes to express his appreciation to Dr. L. W. Schroeder, his adviser, for the suggestion of the topic, and whose invaluable guidance and encouragement have been most helpful during this entire investigation and in the preparation of this thesis.

Likewise, the author wishes to thank Dr. J. C. Evans of Kansas State University for the use of his unpublished computer programs utilized in this study.

Similarly, the author acknowledges Dr. L. W. Schroeder, Dr. J. C. Evans and Mr. T. M. Jordan for the tracings and spectrograms of Beta Coronae Borealis, made at Kitt Peak National Observatory, used in this study and to T. M. Jordan for permission to use certain data from his thesis.

Next, the author acknowledges that the financial support for the use of the computer was provided by the Oklahoma State University Research Foundation.

Also, the author wishes to acknowledge the guidance and counseling of his graduate committee, Dr. L. W. Schroeder, Dr. E. E. Kohnke, and Dr. D. L. Rutledge, during his entire graduate education.

In addition, the author wishes to express sincere gratitude to his parents for their interest and encouragement at all times during his educational career. The author would like to express appreciation to his sons, Ryan and Chris, for their understanding and sacrifice

during this study. Finally, the author would like to express his appreciation and thanks to his wife, Niki, for her interest, encouragement, understanding, and sacrifice that has made this investigation possible. To her I owe an eternal debt.

## TABLE OF CONTENTS

Chapter	Page
I. INTRODUCTION. . . . .	1
Introduction to the Topic. . . . .	1
The Purpose of the Study . . . . .	2
Previous Investigation of Beta Coronae Borealis. . .	3
II. OBSERVATIONAL MATERIAL. . . . .	5
The Spectrograms . . . . .	5
The Intensity Tracings . . . . .	9
Location of the Continuum. . . . .	9
Approximation of the Profiles. . . . .	11
Identification of the Lines. . . . .	11
Determinations of Equivalent Widths. . . . .	11
Explanation of the Equivalent Width Tables . . . . .	15
III. THE CURVE OF GROWTH . . . . .	26
Definition . . . . .	26
The Intensity of an Absorption Line. . . . .	26
The Number of Absorbing Atoms. . . . .	26
Observed Curves of Growth. . . . .	27
Theoretical Curves of Growth. . . . .	28
IV. RESULTS . . . . .	29
Observed Relations Between Measured Quantities . . .	30
The Microturbulence Analysis . . . . .	52
V. SUMMARY AND CONCLUSIONS . . . . .	62
The Turbulence Model . . . . .	62
The Abundances . . . . .	62
Possible Future Research Projects. . . . .	64
SELECTED BIBLIOGRAPHY . . . . .	67

LIST OF TABLES

Table	Page
I. Data for 84-Inch Coude Spectrograph. . . . .	6
II. Data for Microphotometer (D2829, D2836, D2837) . . . . .	9
III. Line Intensities for Neutral and Singly Ionized Chromium in Beta Coronae Borealis . . . . .	17
IV. Line Intensities for Neutral, Singly, and Doubly Ionized Iron in Beta Coronae Borealis. . . . .	18
V. Actinide Line Intensities in Beta Coronae Borealis . . . . .	20
VI. Intensities of Magnetically Sensitive Lines in Beta Co- ronae Borealis . . . . .	41
VII. Intensities of Magnetic Null Lines of Astrophysical In- terest in Beta Coronae Borealis. . . . .	43
VIII. Observed Line Profile Data for Singly Ionized Iron in Beta Coronae Borealis. . . . .	48
IX. Comparison of Various Log gf Values for Neutral Iron Transitions. . . . .	57
X. Abundance Results. . . . .	58
XI. Abundance Result Comparison. . . . .	65

LIST OF FIGURES

Figure	Page
1. Scale Drawing of a Small Section of an Intensity Tracing. . . . .	10
2. The Equivalent Width, $W$ , of a Spectral Line. . . . .	13
3. Measured Line Parameters . . . . .	13
4. Comparison of Observed Equivalent Widths on Different Tracings . . . . .	14
5. Observed Correlation Between $\log h$ and $\log W$ . . . . .	32
6. Observed Relation Between $\log W$ ( $\text{m}\text{\AA}$ ) and $d_c$ ( $r_c$ ) . . . . .	33
7. Observed Relation Between $\log W/\lambda$ and $\log W$ ( $\text{m}\text{\AA}$ ) . . . . .	34
8. Observed Relation Between $\log W$ ( $\text{m}\text{\AA}$ ) and $\log h/\lambda$ . . . . .	35
9. Observed Relation Between $\log W/\lambda$ and $d_c$ ( $r_c$ ) . . . . .	36
10. Observed Relation Between $\log h$ ( $\text{m}\text{\AA}$ ) and $d_c$ ( $r_c$ ) . . . . .	37
11. Observed Relation Between $\log h$ ( $\text{m}\text{\AA}$ ) and $\log W/\lambda$ . . . . .	38
12. Observed Relation Between $\log h$ ( $\text{m}\text{\AA}$ ) and $\log h/\lambda$ . . . . .	39
13. Observed Relation Between $\log h/\lambda$ and $d_c$ ( $r_c$ ) . . . . .	40
14. Observed Curve of Line Width Using Null and Magnetically Sensitive Lines . . . . .	45
15. Magnetic Intensification Using Null and Magnetically Sensitive Lines. . . . .	46
16. Observed Saturation Curve Using Null and Magnetically Sensitive Lines. . . . .	47
17. Observed Profiles of the Magnetically Sensitive Line $\lambda 4202.03$ and the Line $\lambda 4219.36$ of Singly Ionized Iron. . . . .	49
18. Observed Profiles of Two Null Lines of Singly Ionized Iron . . . . .	50

LIST OF FIGURES (continued)

Figure	Page
19. Observed Profiles of the Magnetically Sensitive Line $\lambda 4045.82$ and the Line $\lambda 4199.10$ of Singly Ionized Iron . . . . .	52
20. Theoretical Curve of Growth for Neutral Iron with the Labeled Microturbulent Velocities. . . . .	53
21. Observed Relation Between $\log W/\lambda$ and $\log h/\lambda$ for Beta Coronae Borealis . . . . .	55
22. Theoretical Curve of Growth for Fe I . . . . .	60
23. Empirical Curve of Growth for Fe I . . . . .	60
24. Theoretical Curve of Growth for Cr II. . . . .	61
25. Empirical Curve of Growth for Cr II. . . . .	61



## CHAPTER I

### INTRODUCTION

#### Introduction to the Topic

Abundance determinations from stellar spectra have long preoccupied investigators in the field of astrophysics. The value of abundance determinations lies in the clues which they give to the history of stellar matter. The importance of stellar abundance determinations has been stated by A. Unsöld (1969) of volume 163 of Science, page 1015.

Spectroscopic determinations of the abundances of the chemical elements in stellar atmospheres provides us with the most important indications on stellar evolution. In the vast majority of 'normal' stars the chemical composition of the outer layers is, it turns out, unaffected by the energy-producing nuclear processes in the stellar interior. The composition of the atmosphere of such stars therefore gives us information on the composition of the interstellar matter out of which they originated.

There are, however, rare kinds of stars with atmospheres of highly anomalous composition--the helium-, barium-, carbon-, and 'peculiar' stars, usually designated according to the element whose spectral lines appear strengthened. In such cases we can investigate which nuclear processes were active in transforming the matter that we now observe directly, and we are faced with the problem of explaining how the star managed to 'turn inside out'.

The bearing of abundance determinations on a full understanding of stellar evolution and the nuclear history of the Galaxy is more and more obvious.

Following the discovery of Babcock (1947) that the sharp-lined,

peculiar A-stars have large magnetic fields, several analyses have been made of the spectra of individual stars. In each case the authors agree that the stars have abnormal compositions. This phenomenon is supposed to be purely surface phenomenon which has been brought about by nuclear reactions between particles accelerated in magnetic fields (Burbidge and Burbidge 1955).

The analysis of stellar spectra has developed from the rudimentary curve of growth analysis, the relationship between the width of a line and the number of effective absorbing atoms, first introduced by Minnaert and Slob (1931). Essentially, this technique represents a method for deduction of various atmospheric parameters such as the temperature, pressure and chemical composition, based on the approximation that spectral line formation can be treated as originating in an atmosphere of some fixed temperature and density. An improvement upon the treatment of spectral analysis began with the model technique of Strömgen (1940) and has since been significantly improved by more recent investigations.

#### The Purpose of the Study

The purpose of this study is to determine the preliminary abundances of neutral iron, as well as that of singly ionized chromium, in order to check the probable degree of presence of these elements in the atmosphere of Beta Coronae Borealis. Theoretical curves of growth, observed line profiles, and equivalent widths are utilized to assess the effects of the various line broadening agents present in the atmosphere. In addition, this study will present usable data for selected magnetically sensitive absorption lines, as well as non-splitting absorption lines of iron, chromium, molybdenum, nickel, vanadium, xenon, europium, titan-

ium, and the Actinide-series elements for the purpose of possible future reference.

#### Previous Investigation of Beta Coronae Borealis

This star is peculiar because it has more enhanced lines of europium, chromium, and strontium than the so-called "normal" stars. According to the Henry Draper Catalogue, the right ascension ( $\alpha$ ) and declination ( $\delta$ ) of Beta Coronae Borealis for 1970 are  $\alpha=15^{\text{h}}26^{\text{m}}35^{\text{s}}$  and  $\delta=29^{\circ}12'$ . This peculiar A-star has a photographic apparent magnitude of +3.93, a visual magnitude of 3.7 (Adelman 1973) and a variable color index (B-V) of +0.27 (Abt and Golson 1962). The lines are somewhat broadened by a 6 kilogauss magnetic field with a 18.50 day period and periodic extremes in the effective magnetic field ( $H_e$ ) of +1020 and -960 gauss (Babcock 1963). The solar magnetic field is 1 or 2 gauss and HD 215441 has a 34 kilogauss field, the strongest yet known in nature (Babcock 1958). It is a spectroscopic binary with a period of 3834 days (10.496 years) and an eccentricity of 0.4 (Neubauer 1944; Wolff and Bonsack 1972). Spectroscopic studies reveal that it is not a spectrum variable even though it is a magnetic and light variable (Wolff and Morrison 1971).

The Henry Draper Catalogue classifies Beta Coronae Borealis (HD 137909) as an F0p; Sargent and Searle in 1962 classified it as an A5p (Paschen Type). Beta Coronae Borealis, labeled HR 5747 by the Revised Harvard Photometry Catalogue, is numbered 55 in Babcock's Catalogue of Magnetic Stars (1958) concerning "Stars in which a magnetic field is present."

This Sr-Cr-Eu star has one of the greatest known rare earth abundances (Hack 1958; Hardorp and Shore 1971; Adelman 1973; Shore and

Hardorp 1974) and is the brightest example of a sharp-lined cool magnetic Ap star with an apparent rotational velocity  $\leq 3$  kilometers per second (Adelman and Shore 1973; Preston 1971).

One of the more definitive line identifications lists which covered the spectral region  $\lambda\lambda 3980-4638$  was prepared by W. A. Hiltner (University of Michigan) in 1945 by a short-screw measuring engine directly on the spectrogram. Extended identification lists were made by J. D. Gruber (1972) including the spectral region  $\lambda\lambda 3613-4863$  and T. M. Jordan (1974) including the spectral region  $\lambda\lambda 3400-6953$  (both of Oklahoma State University). Such lists are necessary in order to make a fine analysis abundance determination of various elements in the peculiar A-star, Beta Coronae Borealis.

## CHAPTER II

### OBSERVATIONAL MATERIAL

#### The Spectrograms

Using the Bausch and Lomb (No. 33-53-36-35) grating, the spectrograms were made at the coudé focus of the Kitt Peak National Observatory 84-inch telescope in June of 1971 by Dr. Leon Schroeder and Dr. Ronald Oines both of Oklahoma State University, and Dr. John Evans of Kansas State University. The Kitt Peak National Observatory, which is located 40 miles southwest of Tucson, Arizona and 6875 feet above sea level, is operated by the Association of Universities for Research in Astronomy, Inc. (AURA), under contract with the National Science Foundation. Instrumental data concerning the spectrograph, grating and camera used in recording the stellar spectrograms are contained in Table I.

The spectrograms are about  $1350\text{\AA}$ ,  $1525\text{\AA}$ , and  $3050\text{\AA}$  wide depending on the respective photographic plate dispersions of  $2.25\text{\AA}/\text{mm}$ ,  $2.25\text{\AA}/\text{mm}$ , and  $4.54\text{\AA}/\text{mm}$ . Each 28-inch photographic plate was divided into two 10-inch segments and one 8-inch segment. The first 28-inch plate (D2829) contains the absorption spectrum from about  $3600\text{\AA}$  to about  $4950\text{\AA}$ . The second plate (D2836) contains the absorption spectrum from about  $3900\text{\AA}$  to about  $6950\text{\AA}$  and the last plate (D2837) contains the absorption spectrum from about  $3400\text{\AA}$  to about  $4925\text{\AA}$ .

TABLE I  
 DATA FOR 84-INCH COUDE SPECTROGRAPH

Plate D2829:

Slit Width: 0.075 millimeter

Decker Dimensions: Decker 9

Stellar length: 1.16 millimeter or 3.6 seconds  
 Comparison length (inner): 1.78 millimeter  
 Comparison length (outer): 5.29 millimeter

Grating "C":

Bausch and Lomb No. 33-53-36-35, ruled with two diamonds  
 Ruled area: 204 x 254 millimeter  
 Grooves per millimeter: 600  
 Blaze:  $8000\text{\AA}$  (1st order)  
 Ghost intensity: 0.06% of parent line

Camera: 6

Grating tilt: 7935	f-ratio: f/16
Plate position: 46.0	Focal length: 143.8 inches
Central wavelength: $4400\text{\AA}$	Demagnification from slit to plate: 1.88
Focus: 60.60	Dispersion (2nd order blue): $2.2\text{\AA}/\text{mm}$
Tilt: 4.15	Plate width: 27/32 inches
Emulsion: II a-0	Plate length: 28 inches
Exposure meter count: 15988	Starlight exposure time: 39 minutes
Calibration: Sensitometer, 5-74 filter; Neutral density factor x 100; Exposure time 21 minutes	Iron arc comparison exposure time: 10 sec (no filter)
Developer: D-19 for 4 minutes	Temperature in spectrograph room: $61^{\circ}\text{F}$

POSITION OF STAR:

$\alpha(1970) = 15^{\text{h}}26^{\text{m}}35^{\text{s}}$   
 $\delta(1970) = 29^{\circ}12'$

OBSERVING CONDITIONS:

Seeing: 1  
 Trans: 4

TABLE I (Continued)

Plate D2836:Slit Width: 0.075 millimeterDecker Dimensions: Decker 9

Stellar length: 1.16 millimeter or 3.6 seconds

Comparison length (inner): 1.78 millimeter

Comparison length (outer): 5.29 millimeter

Grating "C":

Bausch and Lomb No. 33-53-36-35, ruled with two diamonds

Ruled area: 204 x 254 millimeter

Grooves per millimeter: 600

Blaze: 8000 $\text{\AA}$  (1st order)

Ghost intensity: 0.06% of parent line

CAMERA: 6

Grating tilt: 8056

Plate position: 46.0 (low)

Central wavelength: 5400 $\text{\AA}$ 

Focus: 60.60

Tilt: 4.15

Emulsion: II a-F

Exposure meter count: 50981

Calibration: Sensitometer,  
4-102 filter; Neutral density  
factor x 100; Exposure time  
34 minutes

Developer: D-19 for 4 minutes

f-ratio: f/16

Focal length: 143.8 inches

Demagnification from slit to  
plate: 1.88Dispersion (1st order blue):  
4.4  $\text{\AA}/\text{mm}$ 

Plate width: 27/32 inches

Plate length: 28 inches

Starlight exposure time: 2<sup>h</sup>03<sup>m</sup>Neon arc comparison exposure  
time: 120 secondsIron arc comparison exposure  
time: 10 seconds (no filter)Temperature in spectrograph  
room: 61 $^{\circ}\text{F}$ POSITION OF STAR:

$$\alpha(1970) = 15^{\text{h}}26^{\text{m}}35^{\text{s}}$$

$$\delta(1970) = 29^{\circ}12'$$

OBSERVING CONDITIONS:

Seeing: 0.8-1

Trans: 2-3

Photographic apparent magnitude: +3.93

TABLE I (continued)

Plate D2837:Slit Width: 0.075 millimeterDecker Dimensions: Decker 9

Stellar length: 1.16 millimeter or 3.6 seconds

Comparison length (inner): 1.78 millimeter

Comparison length (outer): 5.29 millimeter

Grating "C":

Bausch and Lomb No. 33-53-36-35, ruled with two diamonds

Ruled area: 204 x 254 millimeter

Grooves per millimeter: 600

Blaze:  $8000\text{\AA}$  (1st order)

Ghost intensity: 0.06% of parent line

CAMERA: 6

Grating tilt: 7949

Plate position: 46.0 (low)

Central wavelength:  $4200\text{\AA}$ 

Focus: 60.60

Tilt: 4.15

Emulsion: II a-0

Exposure meter count: 18574

Calibration: Sensitometer,  
5-74 filter; Neutral density  
factor x 100; Exposure time  
21 minutes

Developer: D-19 for 4 minutes

f-ratio: f/16

Focal length: 143.8 inches

Demagnification from slit to  
plate: 1.88Dispersion (2nd order blue):  
 $2.2\text{\AA}/\text{mm}$ 

Plate width: 27/32 inches

Plate length: 28 inches

Starlight exposure time:  
42 minutesIron arc comparison exposure  
time: 10 seconds (no filter)Temperature in spectrograph  
room:  $61^{\circ}\text{F}$ POSITION OF STAR:

$$\alpha(1970) = 15^{\text{h}}26^{\text{m}}35^{\text{s}}$$

$$\delta(1970) = 29^{\circ}12'$$

OBSERVING CONDITIONS:

Seeing: 0.8-1

Trans: 2-3

Photographic apparent magnitude: +3.93



### The Intensity Tracings

Nine intensity tracings covering the wavelength range  $\lambda\lambda 3400-6959$  were made by T. M. Jordan in May 1972 with the Hilger-Watts Direct Intensity Microphotometer (Model L-470) at Kitt Peak National Observatory Headquarters in Tucson, Arizona at a carriage speed of 0.50 mm/minute resulting in a plate-to-chart magnification of 102.5/1. Table II below gives the pertinent data for the settings on the microphotometer when the tracings were made.

TABLE II

DATA FOR MICROPHOTOMETER (D2829, D2836, D2837)

Reference Current:	0.60 milliamp
Slit Rotation Setting:	28.5
Slit Length Setting:	2.75
Slit Width Setting:	12
Brown Recorder Gear Ratio:	80/40

#### Location of the Continuum

The continuum was drawn directly on the intensitometer tracings as an average of the galvanometer deflections due to the plate grain in the regions between the lines. Figure 1 is a small section of one of the direct intensity tracings (D2829) and shows the location of the continuum. The microphotometer automatically sets the reference level which is displayed as the zero level at the bottom of the tracings.

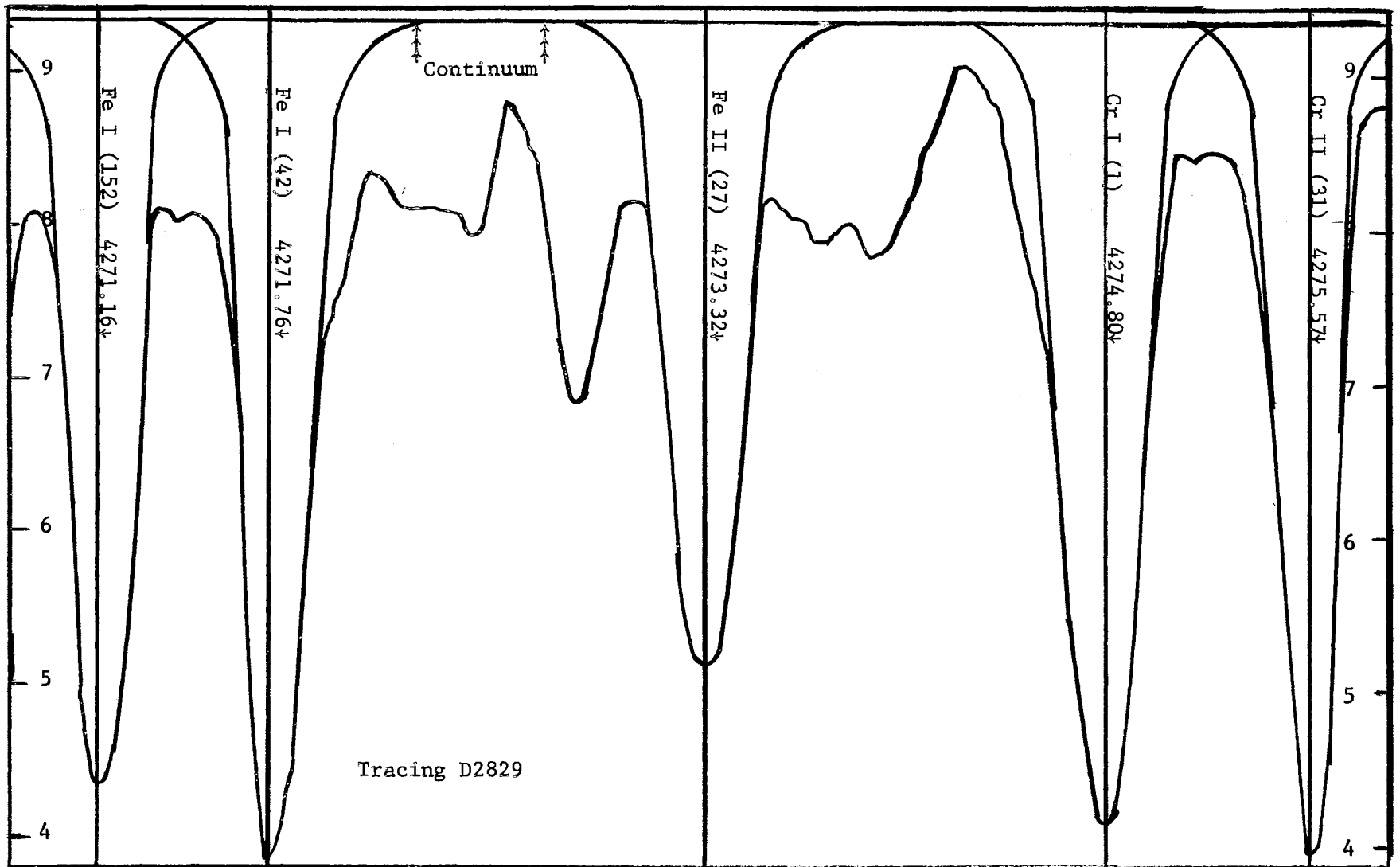


Figure 1. Scale Drawing of a Small Section of an Intensity Tracing

### Approximation of the Profiles

Theory indicated that the shape of the wings exhibited by the stronger lines should be inversely proportional to the square of  $v_D$ , the distance from the line center in units of the Doppler width. An attempt was made to take this into account when drawing the profiles of the stronger lines as shown in Figure 1. The shapes of the wings were readily apparent for very strong lines, especially when there were no nearby lines to produce blending effects in the wings. When blending was serious the wings were roughly approximated.

### Identification of the Lines

The lines were identified by T. M. Jordan (1974) and J. D. Gruber (1972) in their respective theses by various sources: Charlotte E. Moore (1945), A Multiplet Table of Astrophysical Interest, Revised Edition; National Bureau of Standards Monograph 32; MIT Wavelength Tables; Optical Society of America, Journal; National Bureau of Standards Journal of Research; Spectrochimica Acta; Joint Establishment for Nuclear Energy Research; Adelman (1974) and others.

### Determinations of Equivalent Widths

The determination of equivalent widths first involves measurement of the area enclosed by the line profile and the continuum. These areas were obtained using an Ott rolling disc planimeter. The continuum ( $H_c$ ) height was taken as the average of the values adjacent to the line. For each tracing the dispersion was taken at various points along the spectrum and a straight line fitted to a plot of dispersion against wavelength. For the calculation of equivalent widths the dispersion was

then read from these plots. The profile of a line is the plot of the flux at each point in the line versus the wavelength. Hence, the area enclosed by the profile and the continuum is the total amount of energy absorbed in the line. The equivalent width is the width of the rectangle having this same area and with an average height equal to the adjacent continuum. These relations are shown in Figure 2. The equivalent width was calculated in milliangstroms. Due to overlapping and duplication of the spectrograms, some lines were represented by as many as four profiles, a few by only one. The equivalent width, in all cases was taken as the average with all measures assigned equal weight.

Figure 3 displays various measured quantities with respect to the spectral line profiles. These observables are described in the last four paragraphs of the next section concerning the explanation of the table of equivalent width measures. For a representative group of lines Figure 4 compares the equivalent widths measured on different tracings. Theoretically all of the data points in Figure 4 should lie on the straight diagonal line displayed. Since the data points appear to be consistently below this straight line, this suggests that the estimation of the continuum was either slightly too high on tracing D2837 or slightly too low on tracing D2829. Raising the continuum would effectively increase the measured area contained between the profile and the continuum, thus increasing the apparent equivalent width of that spectral line.

Thackeray's (1936) relation was applied to increase the measured equivalent widths of the lines located in the wings of the Balmer lines. This relation is  $W = W_b / r_w$  where  $W_b$  is the measured equivalent width referred to the wing as the continuum,  $r_w$  is the ratio of the intensity

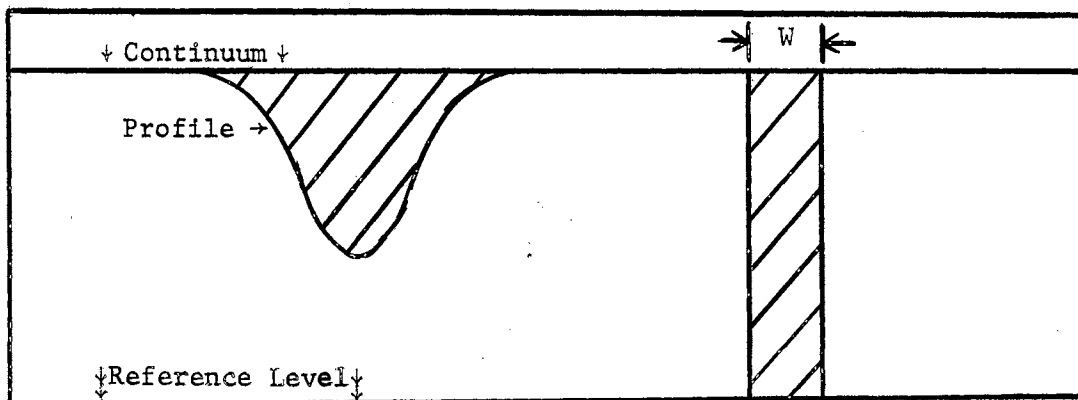


Figure 2. The Equivalent Width,  $W$ , of a Spectral Line

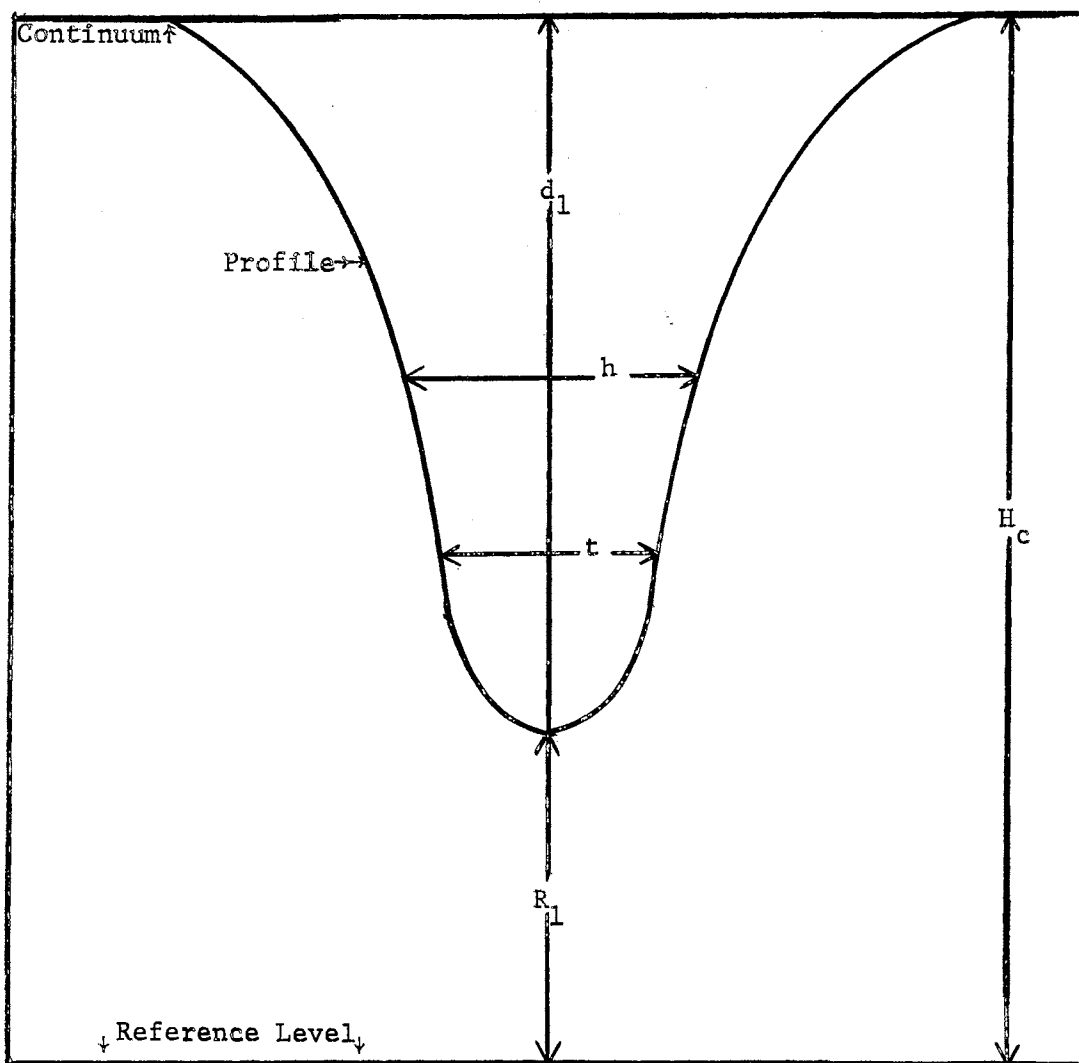


Figure 3. Measured Line Parameters

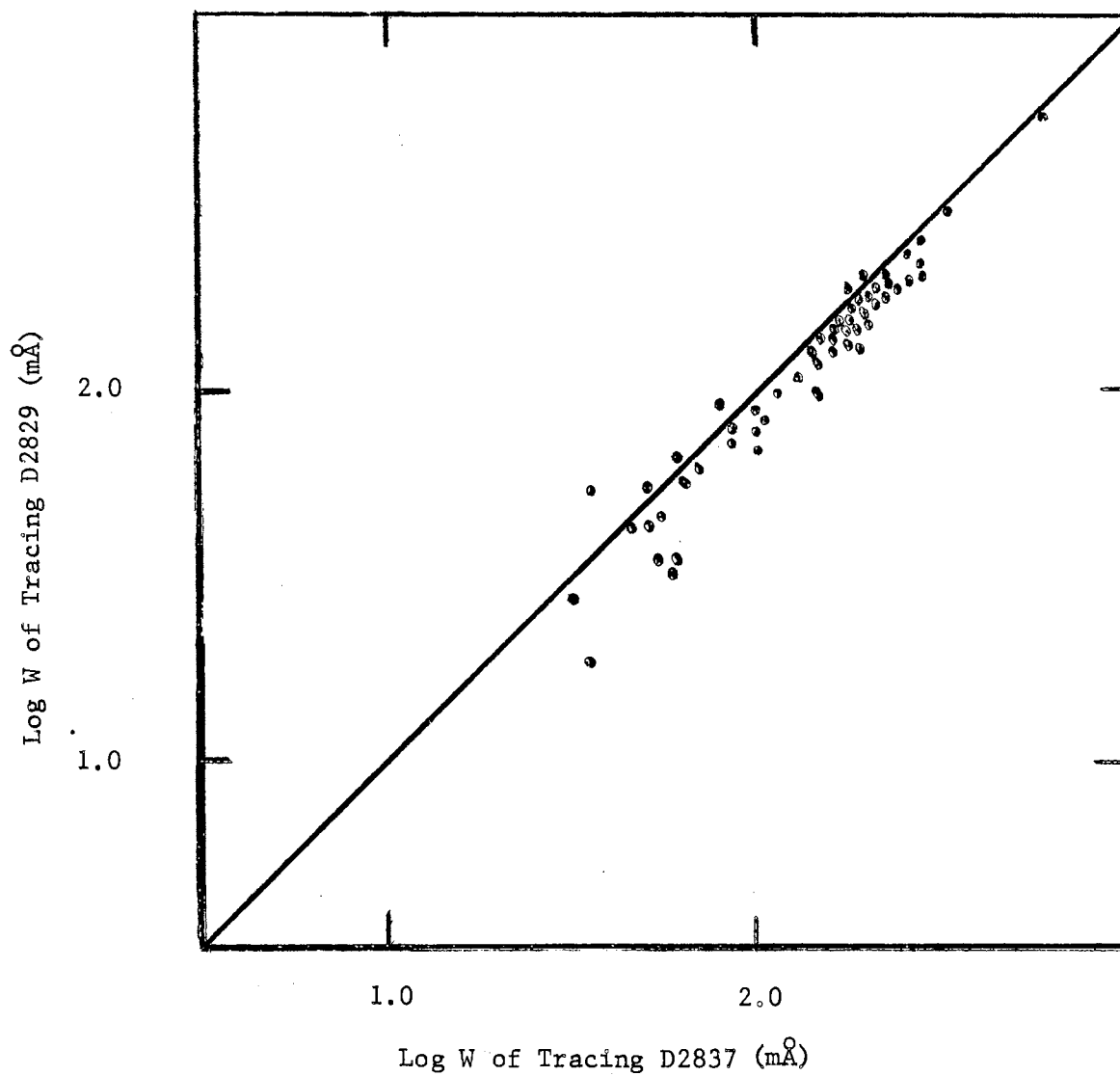


Figure 4. Comparison of Observed Equivalent Widths Measured on Different Tracings

of the wing to the intensity of the true continuum at the center of the line being studied, and  $W$  is the equivalent width the line would have if no blending occurred. This relation is not exact but should be sufficiently accurate to permit the use of such lines.

#### Explanation of the Equivalent Width Tables

Equivalent widths obtained in this study are listed in Tables III, IV and V along with other quantities used in the analysis. A section is included for each element studied, and these are arranged according to increasing atomic weight. Within each section the lines are tabulated in order of increasing wavelength.

Column 1 lists the wavelength in angstroms as given by the source listed in column 3.

Column 2 gives the RMT multiplet number for wavelengths given by Miss Moore (1945) in the Revised Multiplet Table (RMT).

Column 3 lists the source of the wavelength with the following code: R for Moore (1945, 1970); N for National Bureau of Standards Monograph 32; M for the MIT Wavelength Tables; JO for the Optical Society of America, Journal; JENER for the Joint Establishment for Nuclear Research, K1 for Kiess (1951); K3 for Kiess (1953); G6 for Glad (1956); H9 for Humphreys (1939); and S7 for Shenstone (1970).

Column 4 lists the number of profiles measured for the line.

Column 5 gives the equivalent width in milliångstroms. Equivalent widths of lines found in the wings of the Balmer lines have been corrected according to Thackeray's relation.

Column 6 gives the logarithm base ten of the equivalent width in milliångstroms.

Column 7 lists the logarithm base ten of the equivalent width in angstroms divided by the wavelength of the line in angstroms.

Column 8 gives the half width in milli-angstroms.

Column 9 lists the logarithm base ten of the half-width in milli-angstroms.

Column 10 lists the logarithm base ten of the half-width in angstroms divided by the wavelength of the line in angstroms.

Column 11 gives the center line depth as a fraction of the continuum height, i. e.  $d_c = d_1/H_c$ .

Note that  $R_1$  represents the residual line intensity at the line center with respect to the reference level, i. e.  $R_1 = H_c - d_1$ . The elements are arranged in order of increasing ionization and atomic number. In those cases where no ionization is indicated the state has not been determined.



TABLE III

LINE INTENSITIES FOR NEUTRAL AND SINGLY IONIZED  
CHROMIUM IN BETA CORONAE BOREALIS

Wavelength	Multiplet RMT	Source	Number of Measures	W	Log W	Log W/ $\lambda$	h	Log h	Log h/ $\lambda$	$d_c$
Cr I										
3883.66	138	R	0	-	-	-	-	-	-	0.184
3928.16		K3	0	-	-	-	-	-	-	0.220
4251.38		K3	2	20.7	1.32	-5.31	154.0	2.19	-4.44	0.121
4274.80	1	R	3	144.4	2.16	-4.47	366.4	2.56	-4.07	0.573
4749.96		K3	1	20.9	1.32	-5.36	99.7	2.00	-4.68	0.171
4769.80	283	R	0	-	-	-	-	-	-	0.176
4777.73	124	R	0	-	-	-	-	-	-	0.084
4841.73		K3	1	17.6	1.25	-5.44	97.5	1.99	-4.70	0.135
4840.22	266	R	0	-	-	-	-	-	-	0.113
4841.91	266	R	0	-	-	-	-	-	-	0.121
Cr II										
3935.04		K1	0	-	-	-	-	-	-	0.248
4051.97		K1	2	169.3	2.23	-4.38	272.6	2.44	-4.17	0.597
4145.77		K1	2	143.4	2.16	-4.46	272.6	2.44	-4.18	0.508
4179.43		K1	2	253.5	2.40	-4.22	413.1	2.62	-4.01	0.602
4252.62		K1	3	162.9	2.12	-4.42	268.0	2.43	-4.17	0.544
4261.92		K1	3	200.0	2.30	-4.33	338.4	2.53	-4.10	0.575
4275.57		K1	3	146.1	2.17	-4.47	261.7	2.42	-4.21	0.589

TABLE IV  
 LINE INTENSITIES FOR NEUTRAL, SINGLY, AND DOUBLY  
 IONIZED IRON IN BETA CORONAE BOREALIS

Wavelength	Multiplet RMT	Source	Number of Measures	W	Log W	Log W/ $\lambda$	h	Log h	Log h/ $\lambda$	$d_c$
Fe I										
3741.49		M	0	-	-	-	-	-	-	0.298
3767.19	120	R	2	131.5	2.12	-4.46	189.5	2.28	-4.30	0.339
3849.97	20	R	2	170.8	2.24	-4.35	250.1	2.40	-4.19	0.558
3966.53	562	R	1	136.2	2.13	-4.46	226.0	2.35	-4.24	0.250
4045.82	43	R	2	320.3	2.51	-4.10	449.6	2.65	-3.95	0.667
4065.40	698	R	2	64.0	1.81	-4.80	190.0	2.28	-4.33	0.310
4071.74	43	R	2	165.4	2.22	-4.39	261.3	2.42	-4.19	0.600
4137.00	726	R	2	216.3	2.34	-4.28	387.8	2.59	-4.03	0.518
4143.42	523	R	2	155.5	2.19	-4.43	264.1	2.42	-4.20	0.552
4143.87	43	R	2	193.3	2.29	-4.33	328.8	2.52	-4.10	0.595
4150.26	695	R	2	103.5	2.02	-4.60	230.3	2.36	-4.26	0.413
4153.91	695	R	2	247.9	2.39	-4.22	421.5	2.63	-3.99	0.573
4157.79	695	R	2	147.6	2.17	-4.45	297.9	2.47	-4.14	0.476
4187.04	152	R	1	221.8	2.35	-4.28	410.3	2.61	-4.01	0.525
4187.80	152	R	1	317.6	2.50	-4.12	567.6	2.75	-3.87	0.550
4202.03	42	R	3	153.0	2.19	-4.44	265.5	2.42	-4.20	0.572
4210.35	152	R	3	155.4	2.19	-4.43	342.1	2.53	-4.09	0.432
4235.94	152	R	3	187.2	2.27	-4.36	308.4	2.49	-4.14	0.578
4238.82	693	R	3	208.8	2.32	-4.31	375.7	2.58	-4.05	0.562
4250.12	152	R	3	148.6	2.17	-4.46	280.4	2.45	-4.18	0.530
4250.79	42	R	3	188.7	2.28	-4.35	293.5	2.47	-4.16	0.634
4271.16	152	R	3	164.0	2.22	-4.42	297.2	2.47	-4.16	0.584

TABLE IV (continued)

Wavelength	Multiplet RMT	Source	Number of Measures	W	Log W	Log W/ $\lambda$	h	Log h	Log h/ $\lambda$	$d_c$
Fe I (continued)										
4271.76	42	R	3	183.4	2.26	-4.37	301.0	2.48	-4.15	0.600
4282.41	71	R	3	137.7	2.14	-4.49	263.6	2.42	-4.21	0.514
Fe II										
4178.86	28	R	2	210.8	2.32	-4.30	337.2	2.53	-4.09	0.605
4273.32	27	R	3	158.5	2.20	-4.44	342.1	2.53	-4.10	0.458
Fe III										
4263.38		G6	3	42.6	1.63	-5.00	257.9	2.41	-4.22	0.156

TABLE V

## ACTINIDE LINE INTENSITIES IN BETA CORONAE BOREALIS

Wavelength	Multiplet RMT	Source	Number of Measures	W	Log W	Log W/ $\lambda$	h	Log h	Log h/ $\lambda$	d <sub>c</sub>
Ac I										
4613.93		SA	3	38.4	1.58	-5.08	143.9	2.16	-4.51	0.219
4705.77		SA	1	25.7	1.41	-5.26	119.0	2.08	-4.60	0.132
4860.16		SA	0	-	-	-	-	-	-	0.216
Ac II										
3554.99		SA	0	-	-	-	-	-	-	0.432
3565.59		SA	0	-	-	-	-	-	-	0.432
4386.41		SA	1	48.8	1.69	-4.95	244.8	2.39	-4.25	0.200
4605.45		SA	2	45.7	1.66	-5.00	142.7	2.15	-4.51	0.266
Th I										
3754.04		N	1	19.9	1.30	-5.28	90.1	1.96	-4.62	0.087
3765.24		N	1	21.8	1.34	-5.24	129.5	2.11	-4.46	0.080
3803.07		N	1	41.8	1.62	-4.96	157.1	2.20	-4.38	0.201
3898.43		N	0	-	-	-	-	-	-	0.300
3898.50		N	0	-	-	-	-	-	-	0.299
3932.91		N	1	118.9	2.08	-4.52	148.1	2.17	-4.42	0.268
4009.05		N	1	104.4	2.02	-4.58	280.0	2.45	-4.16	0.379
4157.27		N	0	-	-	-	-	-	-	0.181
4157.39		N	1	26.5	1.42	-5.20	172.0	2.24	-4.38	0.157
4170.50		N	2	130.9	2.12	-4.50	363.6	2.56	-4.06	0.314
4214.83		N	2	82.8	1.92	-4.71	322.1	2.51	-4.12	0.227

TABLE V (continued)

Wavelength	Multiplet RMT	Source	Number of Measures	W	Log W	Log W/ $\lambda$	h	Log h	Log h/ $\lambda$	$d_c$
Th I (continued)										
4311.80		N	1	1.4	0.15	-6.49	62.9	1.80	-4.84	0.057
4493.33		N	3	37.2	1.57	-5.08	207.2	2.32	-4.34	0.186
4561.36		N	2	29.7	1.47	-5.19	154.0	2.19	-4.47	0.187
4573.71		N	1	21.8	1.34	-5.32	101.2	2.01	-4.66	0.149
4581.20		N	0	-	-	-	-	-	-	0.235
4695.04		N	3	142.0	2.15	-4.52	631.3	2.80	-3.87	0.230
4723.78		N	2	70.6	1.85	-4.83	239.7	2.38	-4.29	0.232
4808.13		N	1	1.3	0.11	-6.57	55.2	1.74	-4.94	0.083
4822.86		N	1	10.4	1.02	-5.67	97.9	1.99	-4.64	0.080
4852.86		N	2	47.0	1.67	-5.01	121.8	2.09	-4.60	0.200
Th II										
3537.15		N	1	227.6	2.36	-4.19	451.2	2.65	-3.89	0.470
3617.02		N	0	-	-	-	-	-	-	0.394
3617.10		N	0	-	-	-	-	-	-	0.503
3760.28		N	0	-	-	-	-	-	-	0.282
3805.81		N	1	20.0	1.30	-5.28	100.4	2.00	-4.58	0.100
3946.15		N	1	60.2	1.78	-4.82	255.2	2.41	-4.19	0.266
3956.68		N	2	123.8	2.09	-4.50	214.2	2.33	-4.27	0.463
3988.60		N	1	65.3	1.82	-4.79	269.8	2.43	-4.17	0.205
4003.31		N	2	117.0	2.07	-4.53	225.0	2.35	-4.25	0.480
4007.02		N	2	50.8	1.71	-4.90	235.7	2.37	-4.23	0.217
4019.13	3	R	2	43.7	1.64	-4.96	251.8	2.40	-4.20	0.174
4086.52		N	2	44.3	1.65	-4.96	191.1	2.28	-4.33	0.178
4116.71		N	2	63.9	1.81	-4.81	289.2	2.46	-4.15	0.164

TABLE V (continued)

Wavelength	Multiplet RMT	Source	Number of Measures	W	Log W	Log W/ $\lambda$	h	Log h	Log h/ $\lambda$	$d_c$
Th II (continued)										
4148.18		N	2	51.9	1.72	-4.90	238.7	2.38	-4.24	0.223
4178.06		N	2	181.1	2.26	-4.36	470.5	2.67	-3.95	0.376
4179.96		N	1	68.7	1.84	-4.78	337.2	2.53	-4.09	0.203
4229.45		N	3	57.6	1.76	-4.87	190.8	2.28	-4.35	0.275
4274.03		N	2	77.4	1.89	-4.74	387.8	2.59	-4.04	0.202
4281.41		N	1	8.3	0.92	-5.71	103.4	2.02	-4.62	0.075
4328.68		N	1	6.8	0.83	-5.80	89.9	1.95	-4.68	0.058
4485.78		N	2	34.6	1.54	-5.11	215.6	2.33	-4.32	0.178
4575.27		N	1	18.0	1.26	-5.41	84.3	1.93	-4.73	0.053
4694.46		N	0	-	-	-	-	-	-	0.111
4705.76		N	1	23.0	1.36	-5.31	108.0	2.03	-4.64	0.132
4898.80		N	2	28.9	1.46	-5.22	121.5	2.09	-4.61	0.230
Th										
3994.55		N	3	110.3	2.04	-4.56	323.6	2.51	-4.09	0.300
4401.99		N	3	12.3	1.09	-5.55	218.7	2.34	-4.30	0.065
4695.04		N	3	142.0	2.15	-4.52	631.3	2.80	-3.87	0.230
U I										
3926.22		N	1	50.1	1.70	-4.89	258.1	2.41	-4.18	0.162
4042.76		N	2	94.5	1.98	-4.63	309.1	2.49	-4.12	0.271
4556.87		N	2	19.4	1.29	-5.37	109.2	2.04	-4.63	0.140
4576.64		N	1	16.2	1.21	-5.45	118.0	2.07	-4.59	0.128

TABLE V (continued)

Wavelength	Multiplet RMT	Source	Number of Measures	W	Log W	Log W/ $\lambda$	h	Log h	Log h/ $\lambda$	$d_c$
U II										
3670.07		N	1	126.3	2.10	-4.46	271.4	2.43	-4.13	0.230
3831.46		N	2	72.4	1.86	-5.01	160.8	2.21	-4.37	0.217
3854.66		N	0	-	-	-	-	-	-	0.338
3859.58		N	1	111.6	2.05	-4.54	290.5	2.46	-4.12	0.376
3890.36		N	0	-	-	-	-	-	-	0.161
3902.49		N	2	99.2	2.00	-4.60	255.8	2.41	-4.18	0.296
3904.56		N	1	61.8	1.79	-4.80	202.0	2.31	-4.29	0.259
3915.88		N	2	100.0	2.00	-4.59	234.5	2.37	-4.22	0.387
3953.88		N	3	126.3	2.10	-4.50	328.0	2.52	-4.08	0.308
3954.56		N	2	49.8	1.70	-4.90	229.2	2.36	-4.24	0.170
3990.42		N	3	93.6	1.97	-4.64	223.2	2.35	-4.25	0.374
4004.06		N	1	67.3	1.83	-4.77	224.8	2.35	-4.25	0.258
4018.99		N	3	59.5	1.78	-4.83	282.5	2.45	-4.15	0.224
4090.14		N	2	82.4	1.92	-4.70	304.6	2.48	-4.13	0.189
4098.03		N	1	91.9	1.96	-4.65	290.0	2.46	-4.15	0.162
4106.93		N	2	67.1	1.83	-4.79	213.0	2.33	-4.29	0.146
4155.41		N	2	78.4	1.90	-4.72	261.1	2.42	-4.20	0.217
4241.67		N	3	39.0	1.50	-5.04	234.4	2.37	-4.26	0.151
4472.34		N	3	37.9	1.58	-5.07	233.9	2.37	-4.28	0.163
4567.69		N	2	7.3	0.86	-5.66	95.2	1.98	-4.68	0.083
4569.91		N	2	6.6	0.82	-5.84	89.6	1.95	-4.71	0.075
4573.69		N	0	-	-	-	-	-	-	0.126
4646.50		N	1	171.9	2.24	-4.43	381.6	2.58	-4.09	0.453
4722.73		N	2	46.9	1.67	-5.00	391.6	2.59	-4.08	0.183
4858.08		N	1	38.9	1.59	-5.10	83.1	1.92	-4.77	0.230
4859.68		N	2	81.8	1.91	-4.77	102.8	2.01	-4.67	0.342

TABLE V (continued)

Wavelength	Multiplet RMT	Source	Number of Measures	W	Log W	Log W/ $\lambda$	h	Log h	Log h/ $\lambda$	$d_c$
U										
3914.20		N	3	112.6	2.05	-4.54	134.7	2.13	-4.46	0.494
4128.34		N	2	192.0	2.28	-4.33	404.4	2.61	-4.01	0.431
4341.69		JR	1	321.2	2.51	-4.13	472.1	2.67	-3.96	0.651
4700.98		N	1	20.5	1.31	-5.36	88.3	1.95	-4.73	0.135
Np I										
3829.3		JO	0	-	-	-	-	-	-	0.186
3949.2		JO	0	-	-	-	-	-	-	0.313
3988.6		JO	1	65.3	1.82	-4.79	269.8	2.42	-4.17	0.205
4164.5		JO	2	49.4	1.69	-4.93	199.4	2.30	-4.32	0.122
4333.9		JO	0	-	-	-	-	-	-	0.086
Pu II										
3985.47		JENER	2	84.7	1.93	-4.67	211.2	2.33	-4.28	0.328
4021.51		JENER	1	14.7	1.17	-5.44	123.6	2.09	-4.51	0.076
Am I										
4020.25		JO	2	92.6	1.96	-4.64	295.1	2.47	-4.13	0.280
4289.26		JO	0	-	-	-	-	-	-	0.112
Am II										
3562.68		JO	0	-	-	-	-	-	-	0.324



TABLE V (continued)

Wavelength	Multiplet RMT	Source	Number of Measures	W	Log W	Log W/ $\lambda$	h	Log h	Log h/ $\lambda$	$d_c$
Am II (continued)										
3926.25		JO	1	50.1	1.70	-4.89	258.1	2.41	-4.18	0.149
4324.57		JO	2	37.1	1.57	-5.07	151.2	2.18	-4.46	0.171
4445.36		JO	1	8.8	0.94	-5.71	134.9	2.13	-4.52	0.058
4575.59		JO	1	16.0	1.20	-5.46	104.5	2.02	-4.64	0.107
Cm II										
3903.89		JO	2	159.1	2.20	-4.39	247.6	2.39	-4.20	0.540
4024.58		JO	2	194.1	2.29	-4.32	329.4	2.52	-4.09	0.537
4042.75		JO	2	110.3	2.04	-4.56	405.9	2.61	-4.00	0.261
4218.46		JO	3	21.6	1.33	-5.29	168.2	2.23	-4.40	0.118
4240.14		JO	2	14.5	1.16	-5.47	117.4	2.07	-4.56	0.121
4402.52		JO	0	-	-	-	-	-	-	0.134
Bk II										
3752.66		JO	1	40.1	1.60	-4.97	107.0	2.03	-4.55	0.132
Es II										
3547.72		JO	0	-	-	-	-	-	-	0.478

## CHAPTER III

### THE CURVE OF GROWTH

#### Definition

The curve of growth is the relation between the intensity of an absorption line and the number of absorbing atoms active in producing the line.

#### The Intensity of an Absorption Line

The term "intensity" here means the total amount of energy subtracted from the continuous spectrum by the absorption line and is best specified by a quantity called the "equivalent width,"  $W$ , of the line. This quantity is defined in Chapter II.

The advantages of expressing the intensity of a line in terms of the equivalent width are that  $W$  is independent of the Doppler effects of stellar rotation and large scale turbulence in the stellar atmosphere.

#### The Number of Absorbing Atoms

The number of absorbing atoms for a line originating from a level  $n$  and terminating on level  $j$  is given by  $N_n f_{nj}$ , where  $N_n$  is the number of atoms in level  $n$ , and  $f_{nj}$  is the  $f$ -value or oscillator strength of the transition from level  $n$  to level  $j$ . When an atom in level  $n$  is

exposed to radiation of all frequencies it may absorb any one of several different quanta. In specifying the number of effective absorbing atoms for a particular line it is necessary to include the  $f$ -value to take into account the probability of the atom absorbing the particular quantum corresponding to the transition in question. For hydrogen, helium, and other one- and two- electron ions, the  $f$ -values can be quantum mechanically computed. For such complex spectra as those of iron, however,  $f$ -values must be obtained through laboratory experiments.

#### Observed Curves of Growth

Let us consider the growth of a particular line as the number of absorbers is increased. This "growth" of a line may be observed in the laboratory by varying the concentration of the element under investigation in an absorption tube. Lines with strengths depending upon the concentration are formed when light from an incandescent source shines through the tube. The curve of growth shows that, initially, the equivalent width increases linearly with  $N_n f_{nj}$ , and this region is known as the linear portion of the curve. The line becomes progressively deeper in the Doppler core along the linear portion. The curve then begins to level off as the number of absorbers increases further to form what is known as the saturation portion of the curve. The point of departure from linearity is called the "knee" of the curve of growth. In this saturation region, the line broadens primarily in the Doppler core and shows little change in central depth. It is here that the curve is particularly sensitive to temperature and microturbulence (see the paper by Gray and Evans (1973) for a discussion of the sensitivity of the curve of growth to various physical effects).

The effect of different values of microturbulence is shown in Figure 20, Chapter IV. One should note that increasing the microturbulent velocity raises the saturation portion of the curve.

Finally, as the number of absorbers is increased more, the number of atoms is large enough to sufficiently perturb the energy levels so that an appreciable amount of absorption occurs away from the saturation center of the line. The increase in the equivalent width occurs in the damping wings of the line, and the curve begins to turn upwards again. This is known as the damping portion of the curve.

The reliability of the results obtained by the method of curve of growth analysis employed in this study depends strongly upon the number of lines available for the element being investigated. Hence, it was felt that results derived from only a few lines would be of doubtful value. Of the elements studied, singly ionized chromium was represented by five lines; elements with fewer lines available were not considered for analysis.

#### Theoretical Curves of Growth

Calculations of the theoretical curves of growth are based upon various assumptions as to the structure of stellar atmospheres and the mechanism of line formation. For the interested reader, the theory underlying this study may be found in Weem's Ph.D. thesis (1972).

## CHAPTER IV

### RESULTS

The shape and breadth of the Fraunhofer lines in the spectrum of Beta Coronae Borealis are affected by the various line broadening agents. Spectral lines are broadened by a variety of physical mechanisms. Some affect the equivalent width while others do not. The major causes of intrinsically broadened lines are (Aller 1963; van Regemortel 1965):

(a) a Doppler broadening due to random thermal motions of the gas atoms as well as possible small scale mass motion turbulence, in the absorbing atmosphere; (b) radiation or natural broadening, due to the existence of small but finite lifetimes of excited states of a gas atom; (c) Stark broadening, through the influences of electronic field resonance coupling at high densities; (d) Zeeman broadening, due to the relative atomic dipole alignment with the magnetic field; (g) isotopic broadening, a type of pseudo-broadening occurring because of isotopic variations between atoms. The important extrinsic causes for line broadening in stellar spectra are rotational broadening due to contributions to the line from different portions of a rotating stellar surface and large scale turbulent effects in the atmosphere. Beta Coronae Borealis has a slow rotational velocity of less than or equal to three kilometers per second (Adelman and Shore 1973; Preston 1971) and consequently has very sharp lines. This would suggest that the velocity broadening effects would be of negligible importance as compared to the thermal and micro-

turbulence broadening effects.

#### Observed Relations Between Measured Quantities

Figures 5 through 13 contain graphical relations between some of the measured quantities. In the following figures:  $h$  represents the half-width;  $W$  represents the equivalent width;  $d$  represents the center line depth as a fraction of the continuum depth;  $r_c$  represents the residual intensity as a fraction of the continuum depth where  $r_c$  equals  $1 - d_c$ ; and  $\lambda$  represents the wavelength of the spectral line. All measured quantities are displayed in Figure 3, Chapter II, where  $R_1$  represents the residual intensity at the center of the line.

Table VI contains the intensities of some magnetically sensitive lines in Beta Coronae Borealis which were selected from an article by G. W. Preston and D. M. Pyper in the Astrophysical Journal (1965). In Table VII are some magnetic null line intensities of astrophysical interest in Beta Coronae Borealis, which were selected from an article by S. J. Adelman (1973). In Table VI, Table VII, and in Figure 3 and Figures 14 through 16,  $t$  represents the half-half width, which is sometimes called the three-quarter width; and  $z$  represents the  $z$ -value corresponding to the Zeeman effect. The  $z$ -values were also obtained from the 1965 Preston and Pyper paper.

Table VIII consists of data concerning the observed line profiles of six neutral iron lines. Figures 17 through 19 contain the observed profiles of these six iron lines, which could be used to determine the actual macroturbulent velocity in the atmosphere. Note that the macroturbulent velocity does not affect the equivalent width, since by definition it occurs after the line has been formed, and simply rounds

out the line profile. Stars with fairly large macroturbulent velocities tend to have profiles with flat wide bottoms which are raised with respect to the true line depth if no turbulence were present.

The equivalent width was the only observed quantity used in the preliminary abundance analysis. The additional measured quantities, the "by-products" of the measured quantities, were readily measured, calculated and graphed in order to aid possible future research concerning various phenomena in the atmosphere of Beta Coronae Borealis.

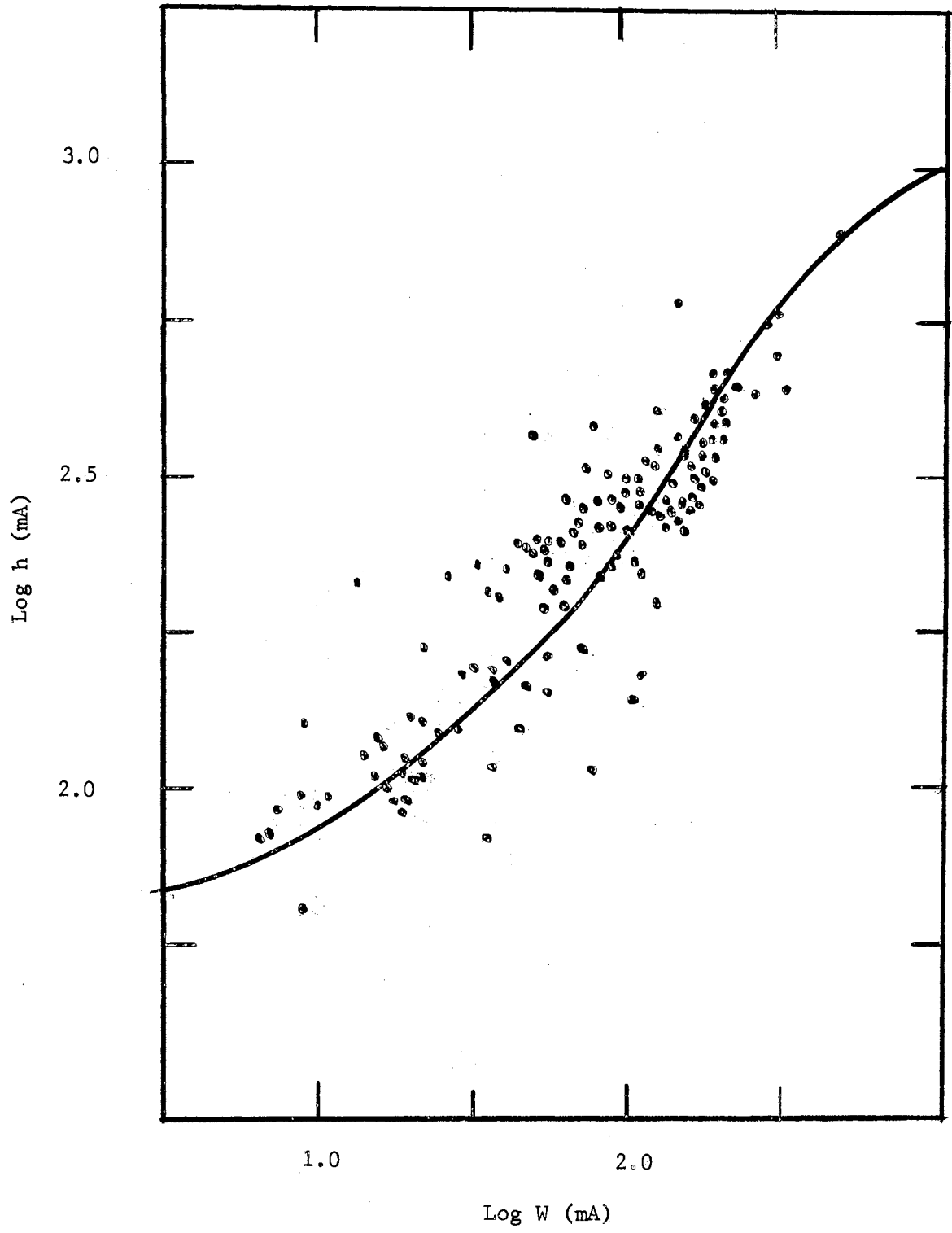


Figure 5. Observed Correlation Between Log h and Log W



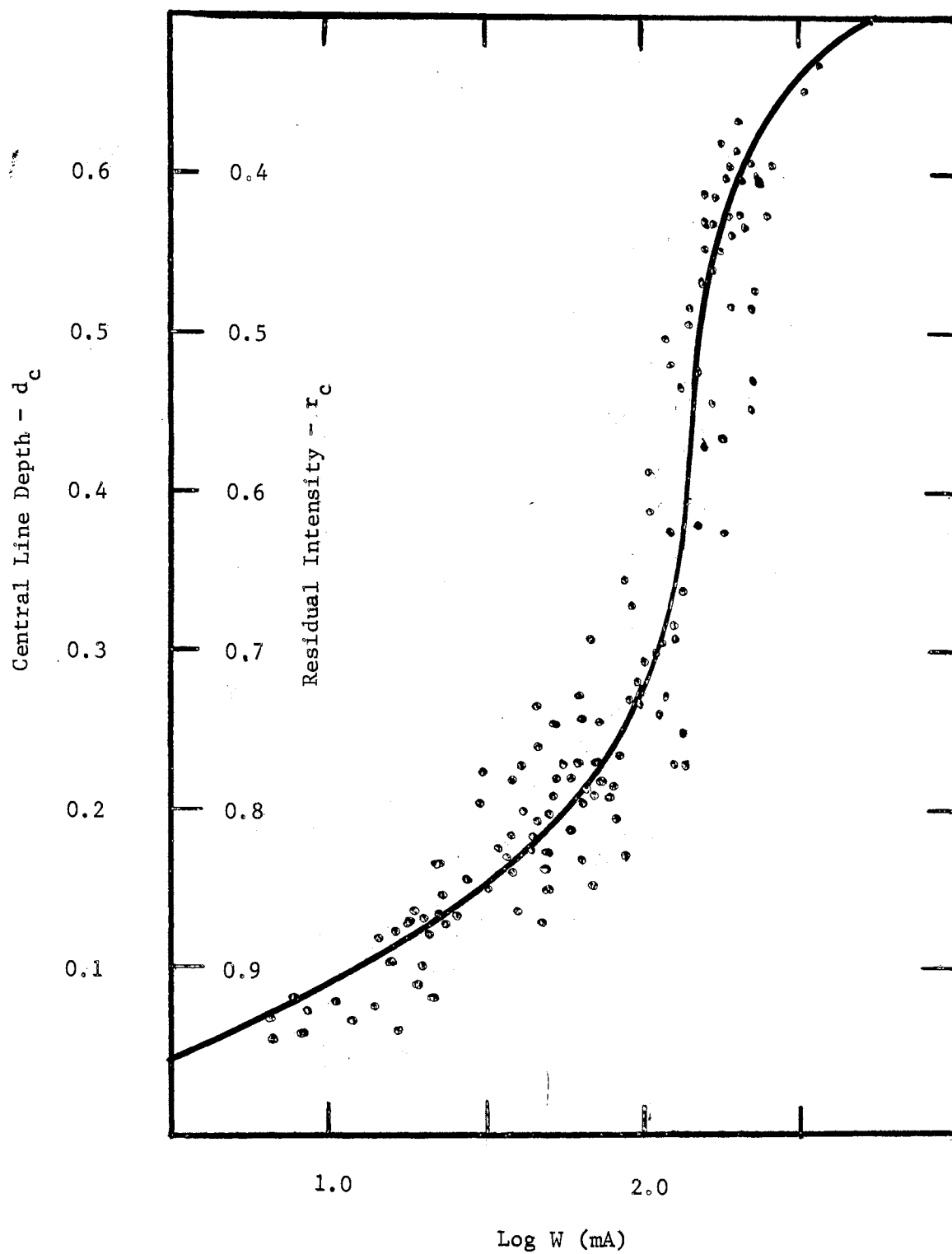


Figure 6. Observed Relation Between Log W (mA) and  $d_c$  ( $r_c$ )

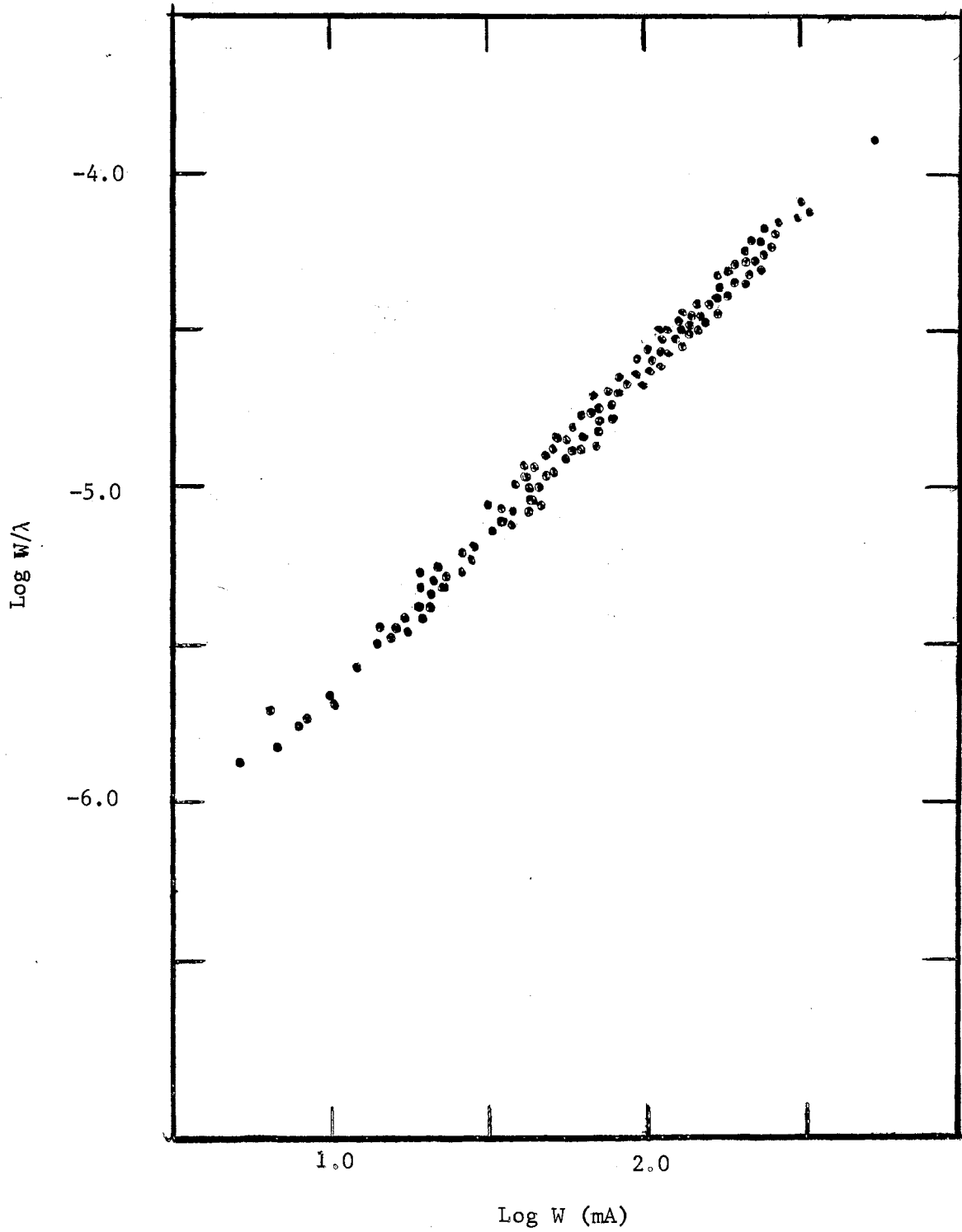


Figure 7. Observed Relation Between  $\text{Log } W/\lambda$  and  $\text{Log } W$  (mA)

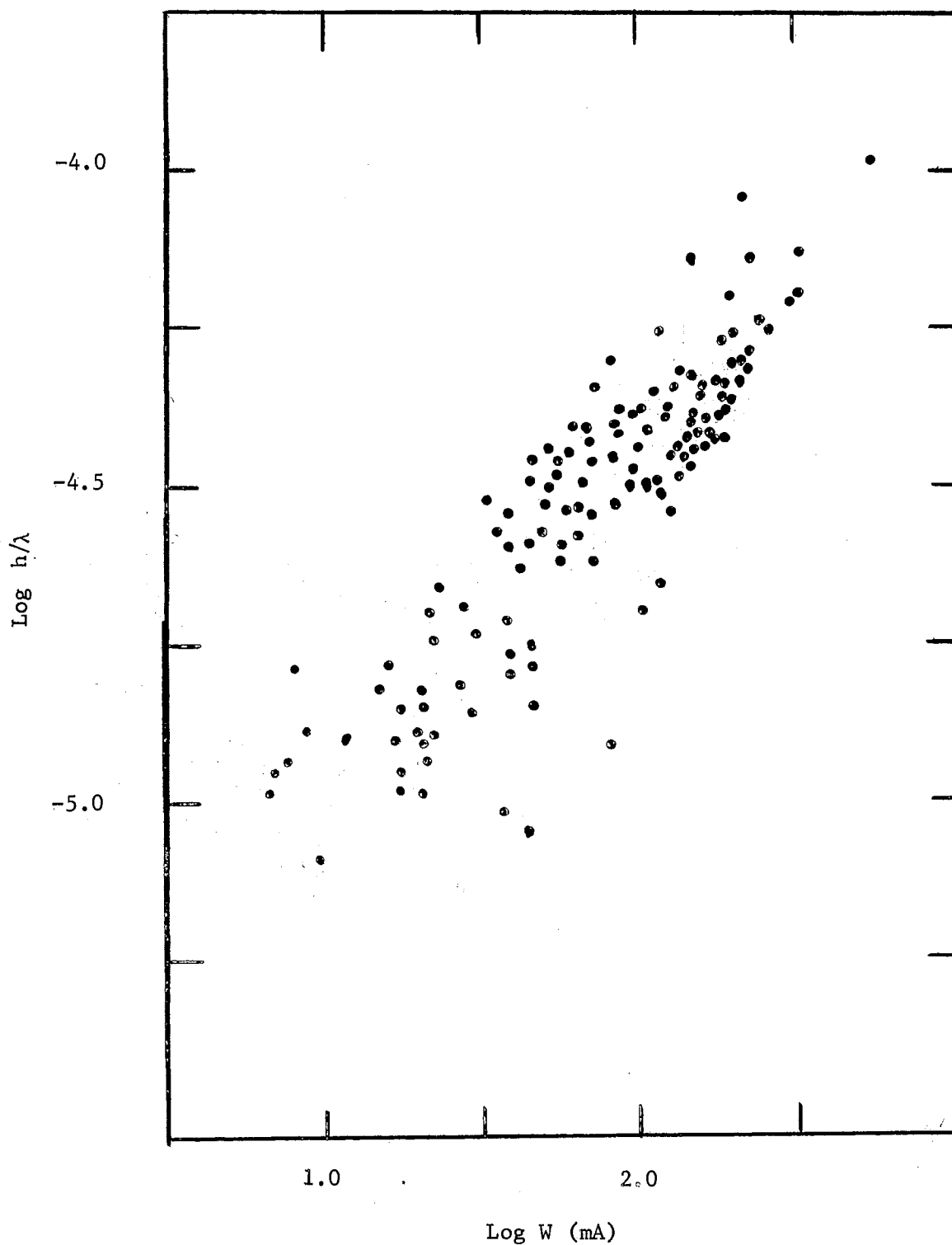


Figure 8. Observed Relation Between  $\text{Log } W$  (mA) and  $\text{Log } h/\lambda$

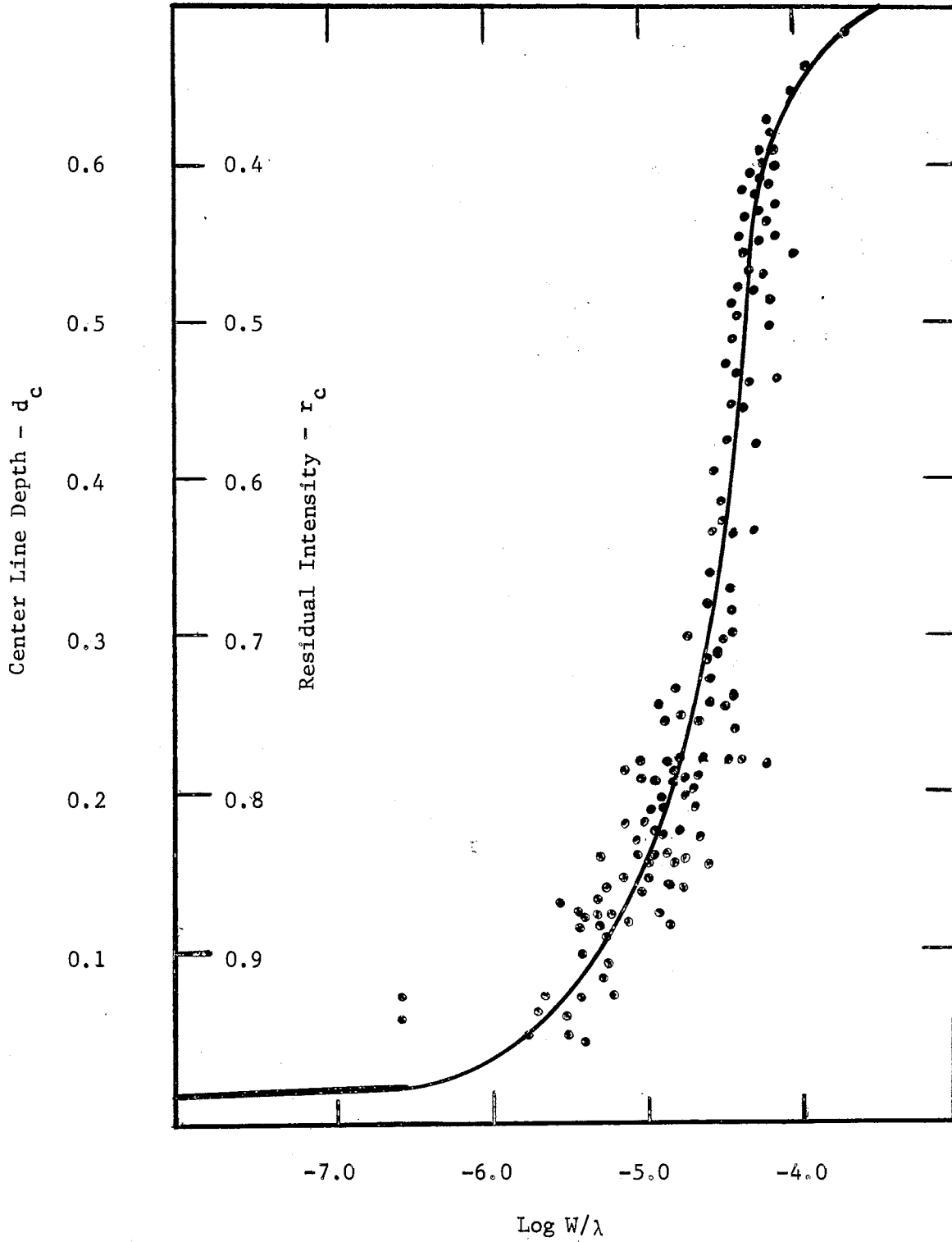


Figure 9. Observed Relation Between  $\text{Log } W/\lambda$  and  $d_c$  ( $r_c$ )

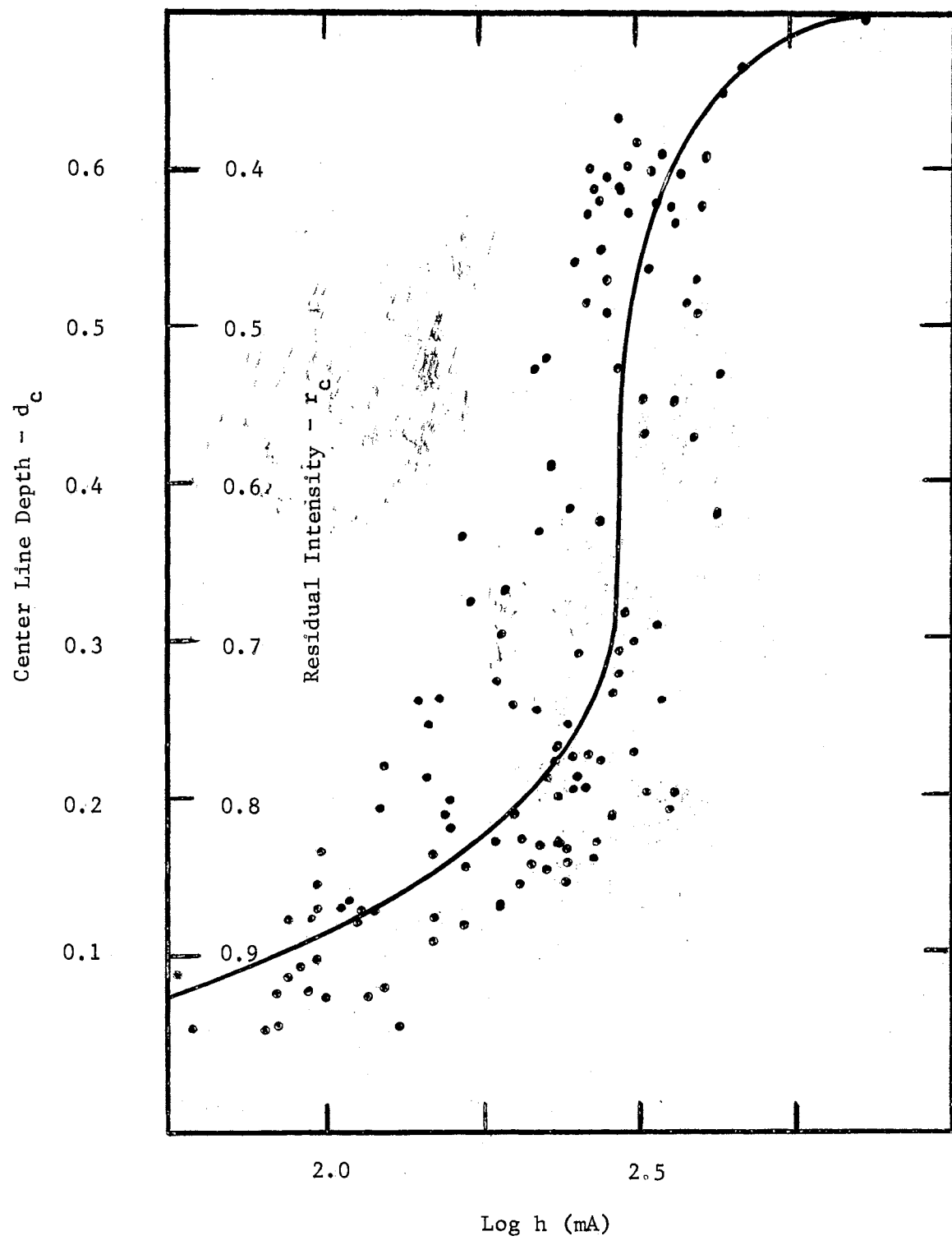


Figure 10. Observed Relation Between Log h (mA) and d<sub>c</sub> (r<sub>c</sub>)

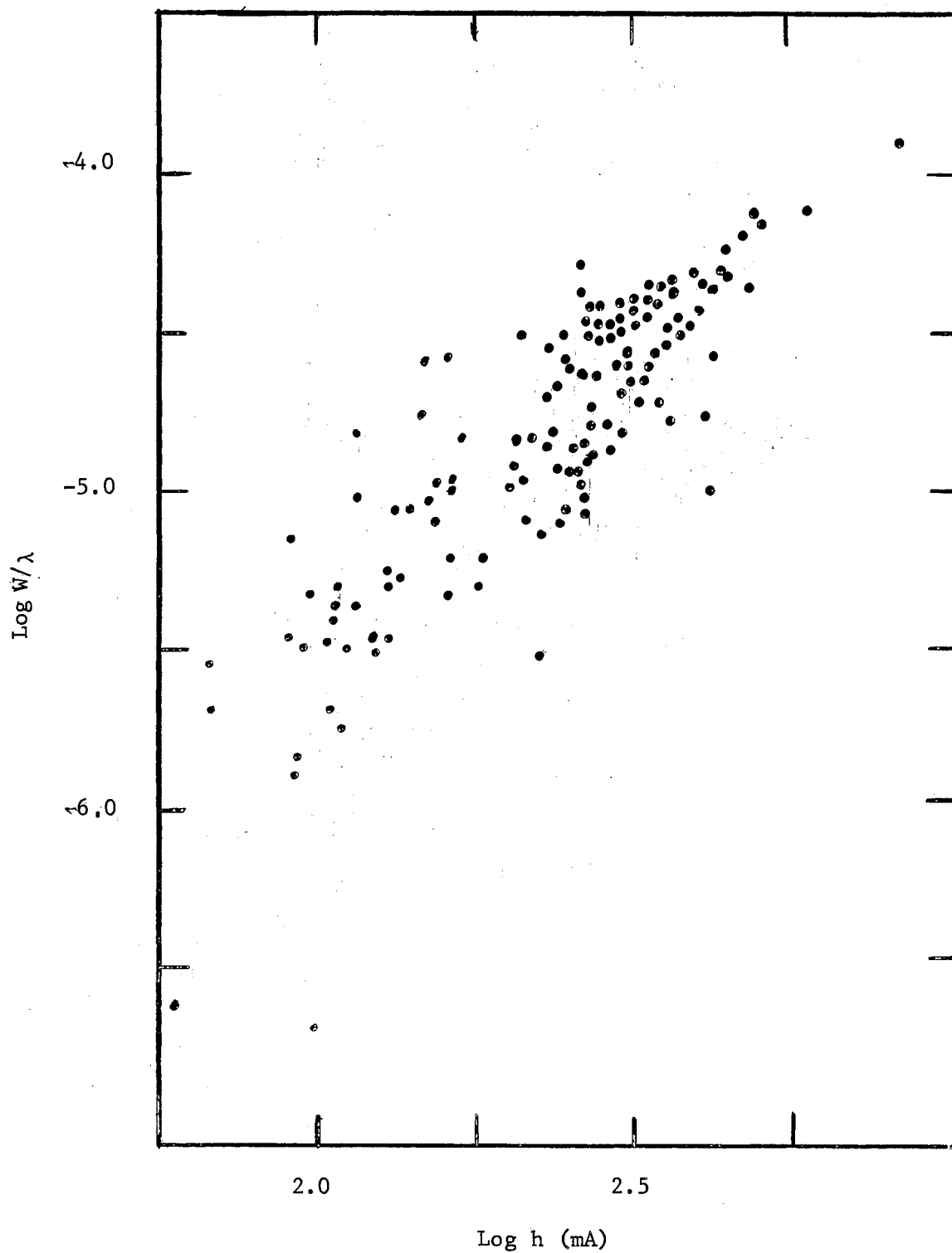


Figure 1]. Observed Relation Between  $\text{Log } h \text{ (mA)}$  and  $\text{Log } W/\lambda$

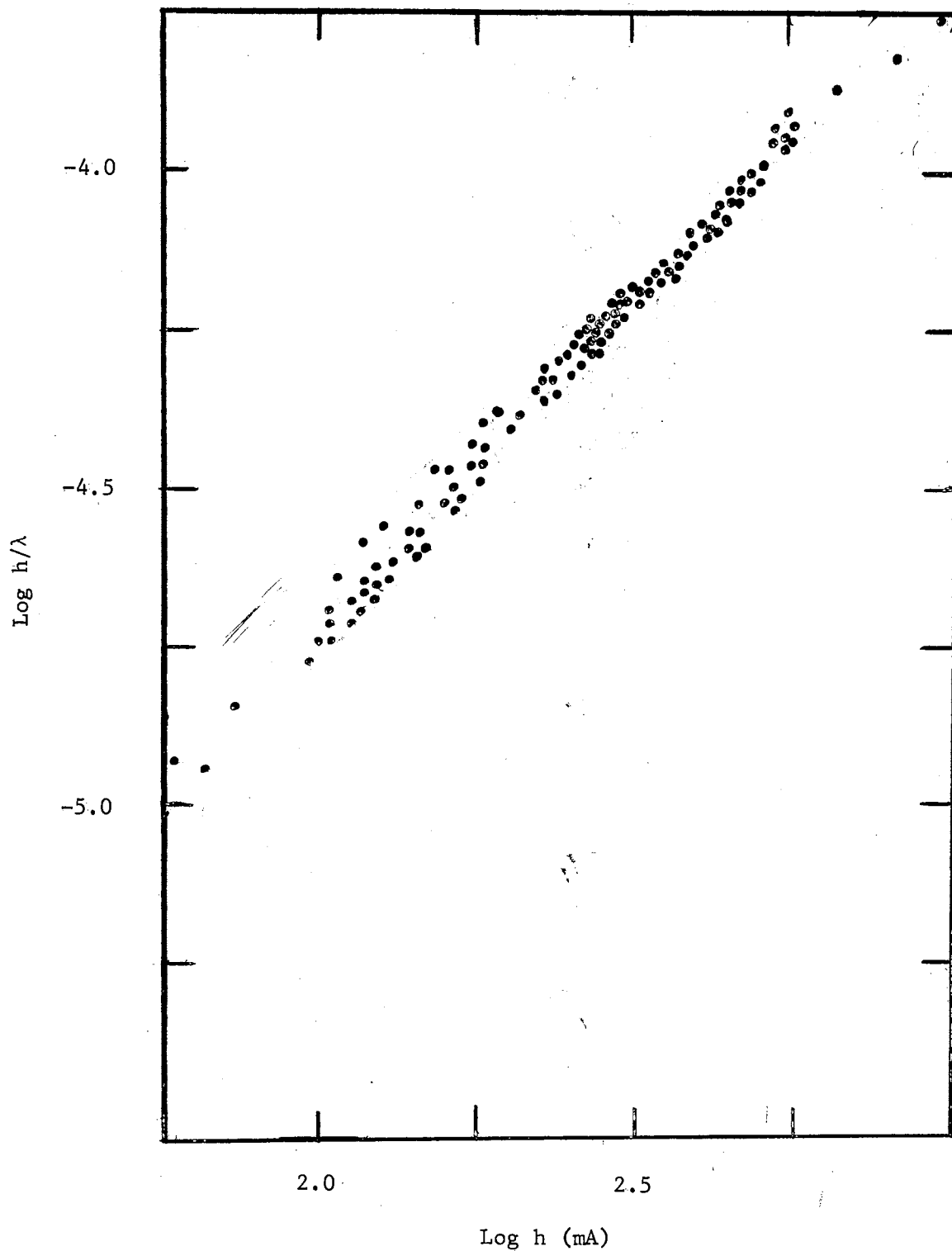


Figure 12. Observed Relation Between  $\text{Log } h/\lambda$  and  $\text{Log } h \text{ (m\AA)}$

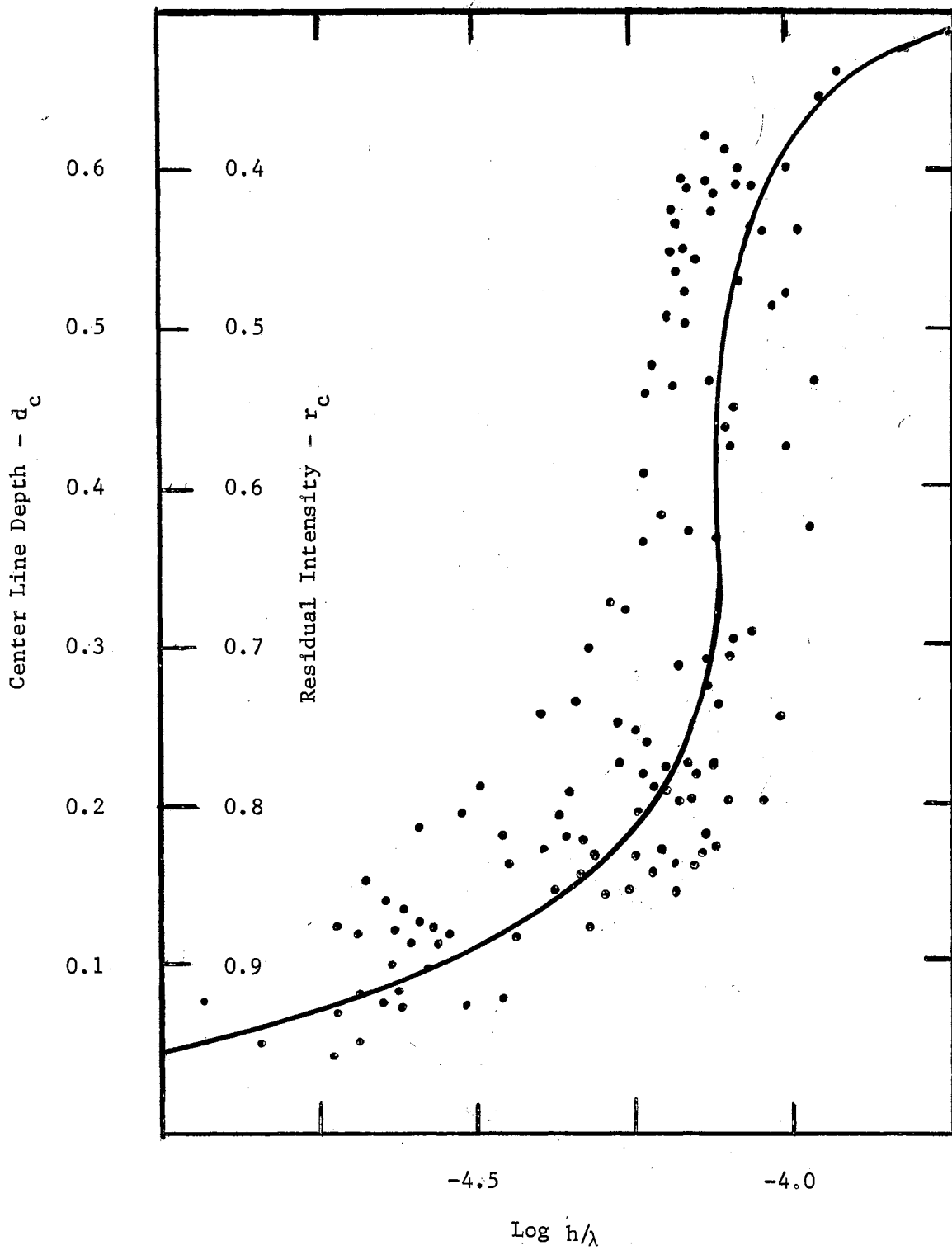


Figure 13. Observed Relation Between  $\text{Log } h/\lambda$  and  $d_c$  ( $r_c$ )



TABLE VI

 INTENSITIES OF MAGNETICALLY SENSITIVE  
 LINES IN BETA CORONAE BOREALIS

$\lambda$	Multiplet RMT	Source and Measures	$z$	$z\lambda$	$W$	$\text{Log } W/\lambda$	$h$	$\text{Log } h/\lambda$	$t$	$t/h$	$r_c$
Ti II											
4163.64	105	R,2	1.07	4455.09	199.2	-4.32	317.5	-4.12	204.8	0.645	0.381
4312.86	41	R,3	1.48	6383.03	221.6	-4.29	370.2	-4.07	236.2	0.638	0.405
Cr I											
4274.80	1	R,3	1.96	8378.61	144.4	-4.47	366.4	-4.07	253.6	0.692	0.427
Cr II											
4051.97		K1,2	1.14	4619.24	169.3	-4.38	272.6	-4.17	179.5	0.659	0.403
4145.77	162	R,2	1.20	4974.92	143.4	-4.46	272.6	-4.18	171.1	0.628	0.492
4179.43		K1,2	1.22	5098.90	253.5	-4.22	413.1	-4.01	291.7	0.706	0.398
4254.62		K1,3	1.20	5103.14	162.9	-4.42	268.0	-4.17	202.0	0.754	0.456
4261.92		K1,3	1.08	4602.87	200.0	-4.33	338.4	-4.10	234.5	0.693	0.425
4275.57	31	R,3	0.90	3848.01	146.1	-4.47	261.7	-4.21	189.6	0.725	0.411
Fe I											
4045.82	43	R,2	1.25	5057.28	320.3	-4.10	449.6	-3.95	260.9	0.580	0.333
4071.74	43	R,2	0.67	2728.07	165.4	-4.39	261.3	-4.19	135.8	0.520	0.400
4137.00	726	R,2	1.00	4137.00	216.3	-4.28	387.8	-4.03	217.9	0.518	0.482
4143.42	523	R,2	1.00	4143.42	155.5	-4.43	264.1	-4.20	175.0	0.663	0.448

TABLE VI (continued)

$\lambda$	Multiplet RMT	Source and Measures	$z$	$z\lambda$	$W$	$\text{Log } W/\lambda$	$h$	$\text{Log } h/\lambda$	$t$	$t/h$	$r_c$
Fe I (continued)											
4143.87	43	R,2	1.50	6215.81	193.3	-4.33	328.8	-4.10	213.2	0.648	0.405
4153.91	695	R,2	1.50	6230.87	247.9	-4.22	421.5	-3.99	255.3	0.606	0.427
4157.79	695	R,2	1.50	6236.69	147.6	-4.45	297.9	-4.14	193.5	0.650	0.524
4187.04	152	R,1	1.50	6280.56	221.8	-4.28	410.3	-4.01	248.0	0.604	0.475
4187.80	152	R,1	1.50	6281.70	317.6	-4.12	567.6	-3.87	336.6	0.593	0.450
4202.03	42	R,3	1.15	4832.33	153.0	-4.44	265.5	-4.20	185.7	0.699	0.428
4210.35	152	R,3	3.00	12631.05	155.4	-4.43	342.1	-4.09	258.1	0.754	0.568
4235.94	152	R,3	1.65	6989.30	187.2	-4.36	308.4	-4.14	223.3	0.724	0.422
4238.82	693	R,3	1.00	4238.82	208.8	-4.31	375.7	-4.05	244.0	0.648	0.438
4250.12	152	R,3	1.50	6375.18	148.6	-4.46	280.4	-4.18	190.7	0.680	0.470
4250.79	42	R,3	0.92	3910.73	188.7	-4.35	293.5	-4.16	213.2	0.726	0.366
4271.16	152	R,3	1.50	6406.74	164.0	-4.42	297.2	-4.16	206.4	0.695	0.416
4271.76	42	R,3	1.10	4698.94	183.4	-4.37	301.0	-4.15	207.6	0.690	0.400
4282.41	71	R,3	1.33	5695.60	137.7	-4.49	263.6	-4.21	218.1	0.827	0.486
Fe II											
4178.86	28	R,2	0.80	3343.09	210.8	-4.30	337.2	-4.09	218.8	0.649	0.395
4273.32	27	R,3	2.17	9273.10	158.5	-4.44	342.1	-4.10	244.6	0.715	0.542
Eu II											
4129.71	1	R,2	1.98	8176.86	519.9	-3.90	750.3	-3.74	454.4	0.606	0.309

TABLE VII  
 INTENSITIES OF MAGNETIC NULL LINES  
 OF ASTROPHYSICAL INTEREST  
 IN BETA CORONAE BOREALIS

$\lambda$	Multiplet RMT	Source and Measures	z	$z\lambda$	W	Log W/ $\lambda$	h	Log h/ $\lambda$	t	t/h	$r_c$
C II											
3969.52	37	R,0	0	0	-	-	-	-	-	-	0.885
V I											
3912.21	42,43	R,0	0	0	-	-	-	-	-	-	0.722
Cr I											
3883.66	138	K3,0	0	0	-	-	-	-	-	-	0.816
3928.16		K3,0	0	0	-	-	-	-	-	-	0.780
4251.38		K3,2	0	0	20.7	-5.31	154.0	-4.44	101.0	0.656	0.879
4749.96		K3,1	0	0	20.9	-5.36	99.7	-4.68	64.8	0.650	0.829
4769.80	283	K3,0	0	0	-	-	-	-	-	-	0.824
4777.73	124	K3,0	0	0	-	-	-	-	-	-	0.916
4841.73	266	K3,1	0	0	17.6	-5.44	97.5	-4.70	65.4	0.671	0.865
4841.91	266	K3,0	0	0	-	-	-	-	-	-	0.887
Cr II											
3935.04		K1,0	0	0	-	-	-	-	-	-	0.752

TABLE VII (continued)

$\lambda$	Multiplet RMT	Source and Measures	z	$z\lambda$	W	Log W/ $\lambda$	h	Log h/ $\lambda$	t	t/h	$r_c$
Fe I											
3741.49		M,0	0	0	-	-	-	-	-	-	0.702
3767.19	120	R,2	0	0	131.5	-4.46	189.5	-4.30	114.4	0.604	0.661
3849.97	20	R,2	0	0	170.8	-4.35	250.1	-4.19	155.6	0.622	0.442
3966.53	562	R,1	0	0	136.2	-4.46	226.0	-4.24	162.7	0.720	0.750
4065.40	698	R,2	0	0	64.0	-4.80	190.0	-4.33	115.6	0.608	0.690
4150.26	695	R,2	0	0	103.5	-4.60	230.3	-4.26	140.3	0.609	0.587
Fe III											
4263.38		G6,3	0	0	42.6	-5.00	257.9	-4.22	123.4	0.479	0.844
Ni II											
4829.49		S7,1	0	0	49.0	-4.93	143.0	-4.53	89.8	0.628	0.746
Mo II											
4267.83		K8,3	0	0	109.5	-4.59	310.3	-4.14	191.3	0.617	0.702
Xe II											
4243.88		H9,1	0	0	9.9	-5.63	61.8	-4.84	38.3	0.620	0.857

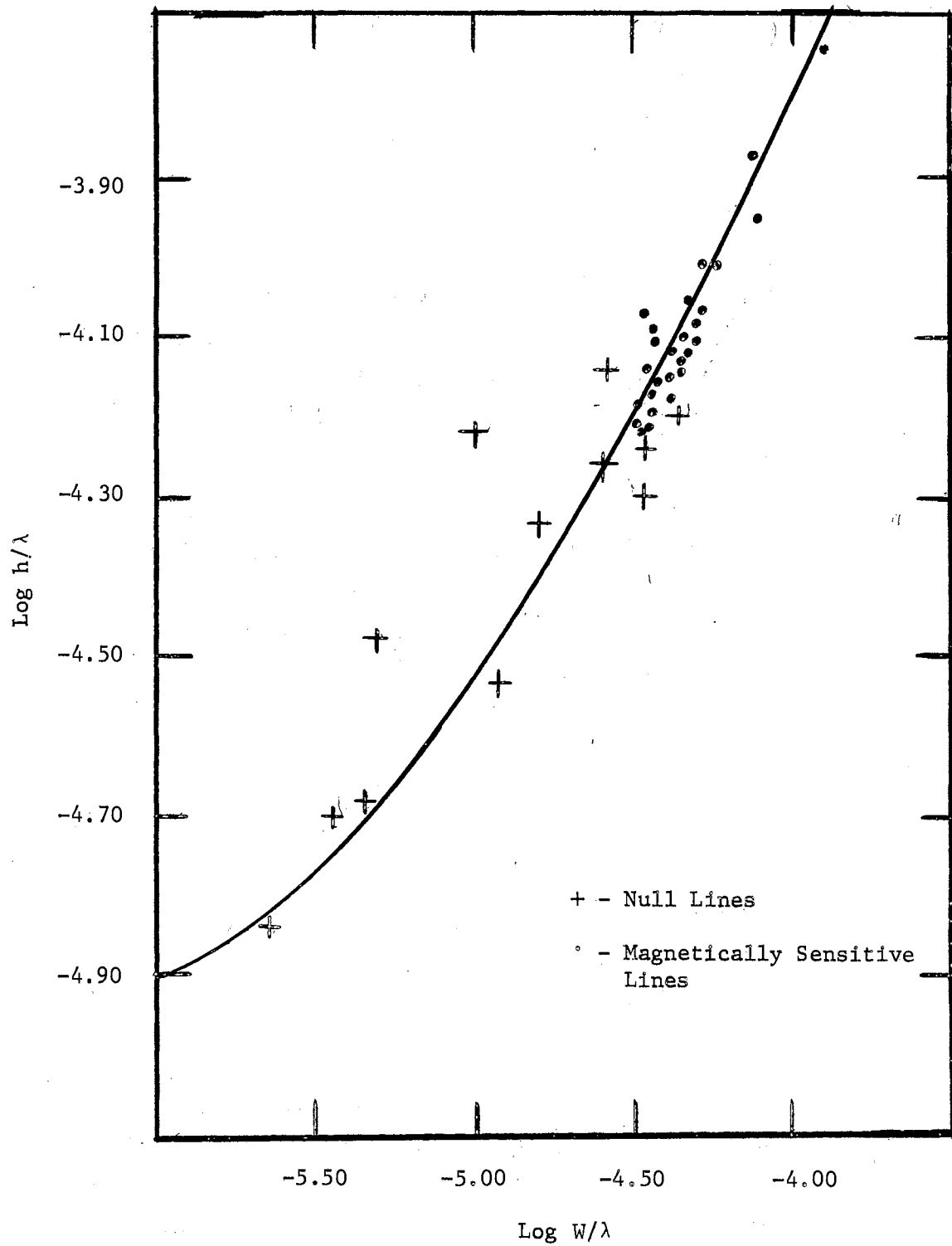


Figure 14. Observed Curve of Line Width Using Null and Magnetically Sensitive Lines

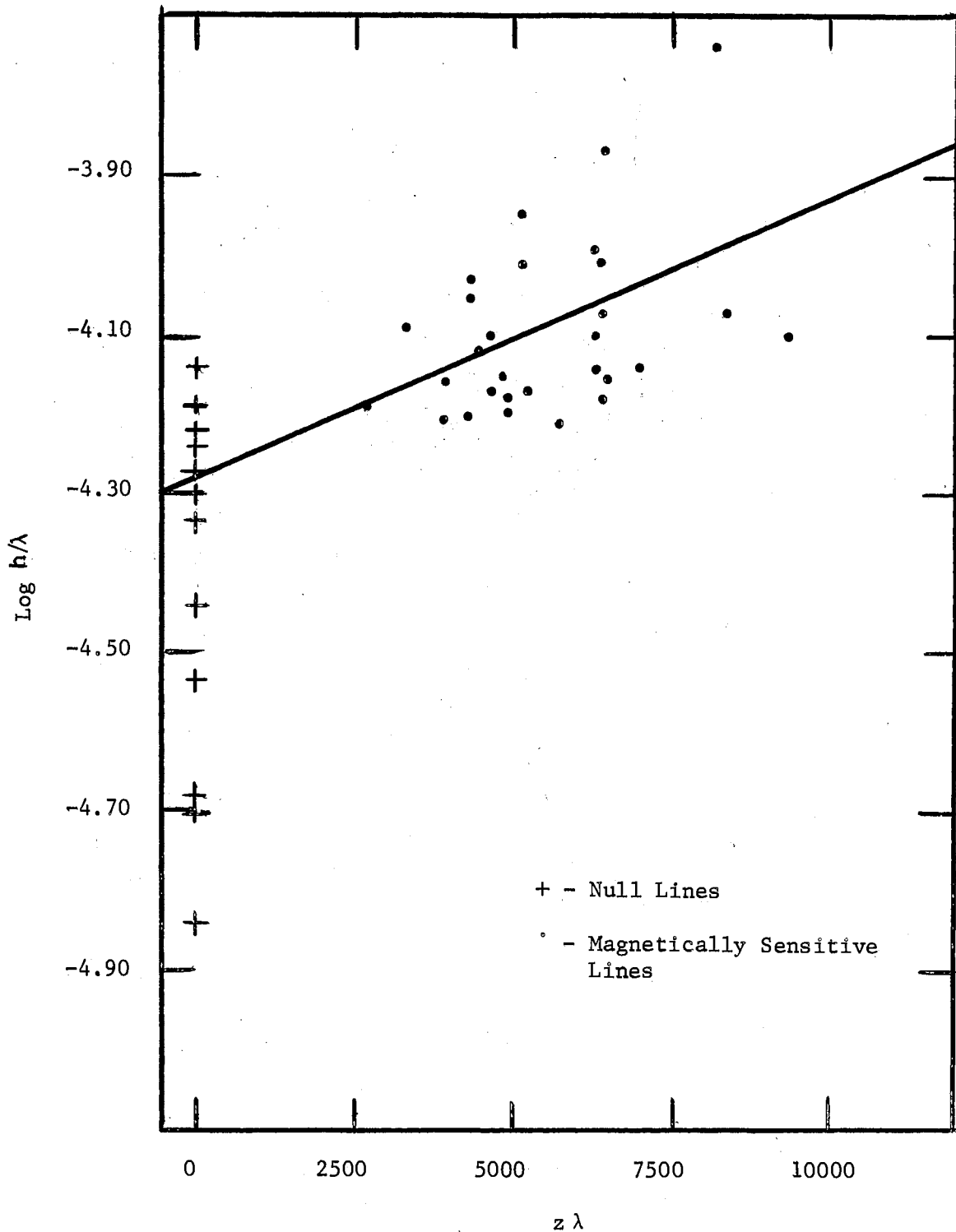


Figure 15. Magnetic Intensification Using Null and Magnetically Sensitive Lines

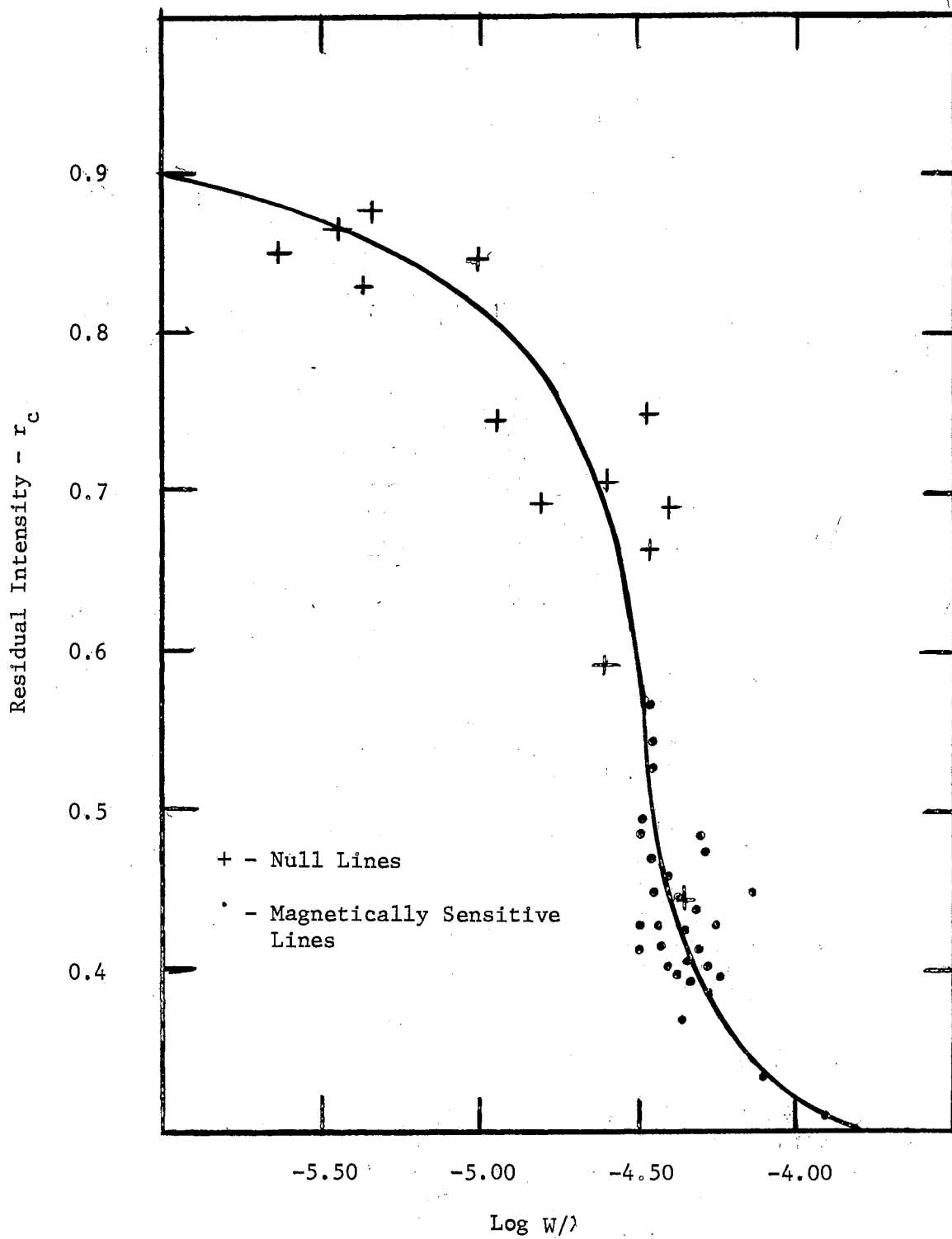


Figure 16. Observed Saturation Curve Using Null and Magnetically Sensitive Lines

TABLE VIII

OBSERVED LINE PROFILE DATA FOR SINGLY IONIZED IRON IN BETA CORONAE BOREALIS

Fe I $\lambda 4045.82$		Fe I $\lambda 4065.40$		Fe I $\lambda 4150.26$		Fe I $\lambda 4199.10$		Fe I $\lambda 4202.03$		Fe I $\lambda 4219.36$	
$\Delta\lambda(\text{\AA})$	Line Depth	$\Delta\lambda(\text{\AA})$	Line Depth	$\Delta\lambda(\text{\AA})$	Line Depth	$\Delta\lambda(\text{\AA})$	Line Depth	$\Delta\lambda(\text{\AA})$	Line Depth	$\Delta\lambda(\text{\AA})$	Line Depth
0.000	0.623	0.000	0.295	0.000	0.390	0.000	0.502	0.000	0.604	0.000	0.526
0.056	0.594	0.028	0.280	0.028	0.377	0.028	0.482	0.028	0.582	0.028	0.526
0.084	0.882	0.056	0.221	0.056	0.328	0.056	0.417	0.056	0.528	0.056	0.441
0.112	0.499	0.084	0.164	0.084	0.278	0.084	0.326	0.070	0.483	0.084	0.369
0.140	0.456	0.112	0.106	0.112	0.189	0.112	0.230	0.084	0.423	0.112	0.271
0.168	0.406	0.140	0.061	0.140	0.140	0.140	0.171	0.112	0.329	0.141	0.183
0.224	0.311	0.168	0.039	0.168	0.101	0.168	0.125	0.140	0.385	0.169	0.113
0.280	0.221	0.224	0.021	0.224	0.051	0.224	0.066	0.168	0.233	0.225	0.054
0.336	0.132	0.280	0.015	0.280	0.033	0.280	0.044	0.196	0.199	0.281	0.029
0.392	0.096	0.336	0.003	0.336	0.020	0.336	0.028	0.224	0.083	0.337	0.014
0.448	0.069	0.392	0.000	0.392	0.015	0.392	0.016	0.280	0.031	0.399	0.000
0.504	0.045			0.476	0.002	0.538	0.000	0.370	0.009		
0.560	0.027			0.504	0.000			0.470	0.000		
0.616	0.017										
0.678	0.000										



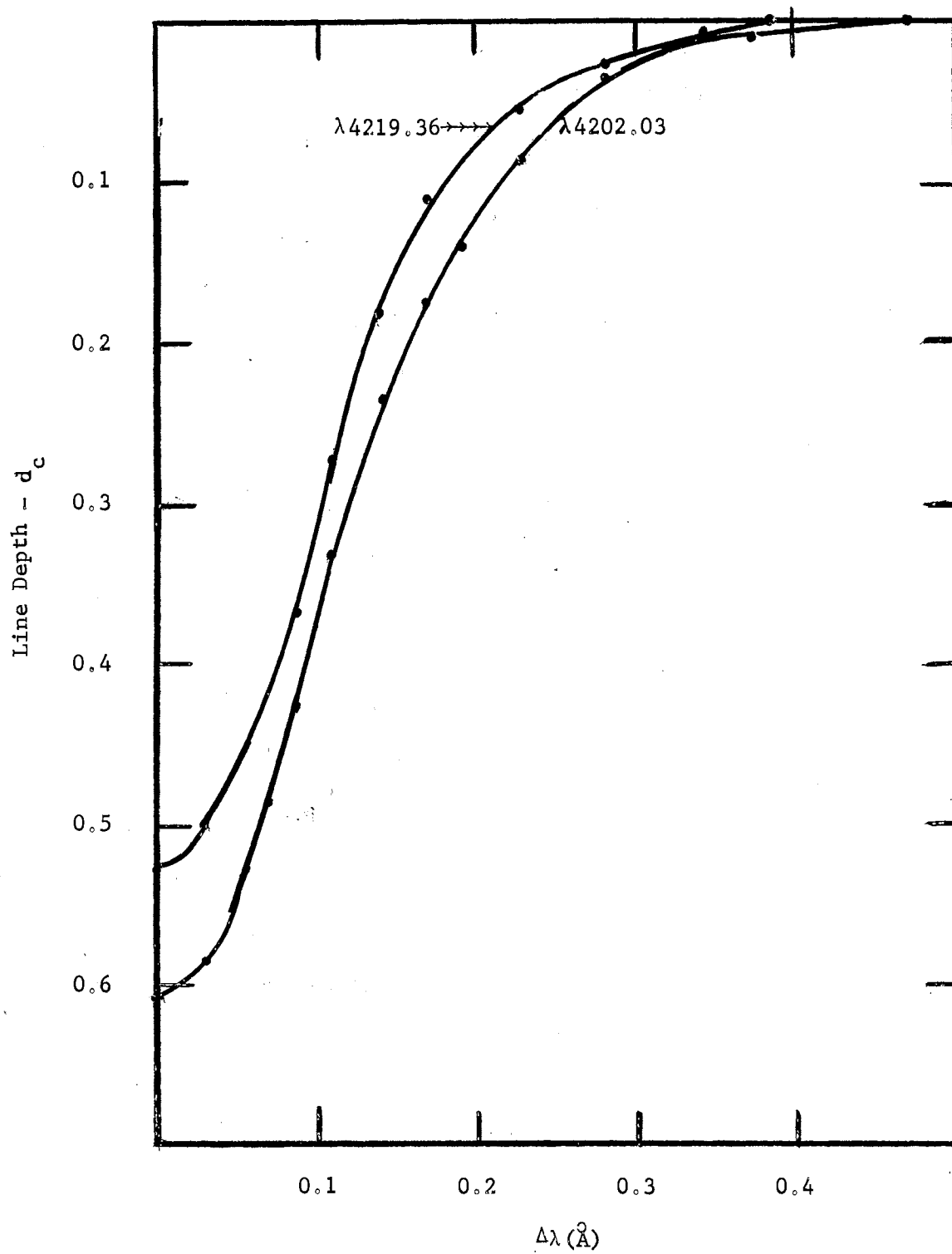


Figure 17. Observed Profiles of the Magnetically Sensitive Line  $\lambda 4202.03$  and the Line  $\lambda 4219.36$  of Singly Ionized Iron

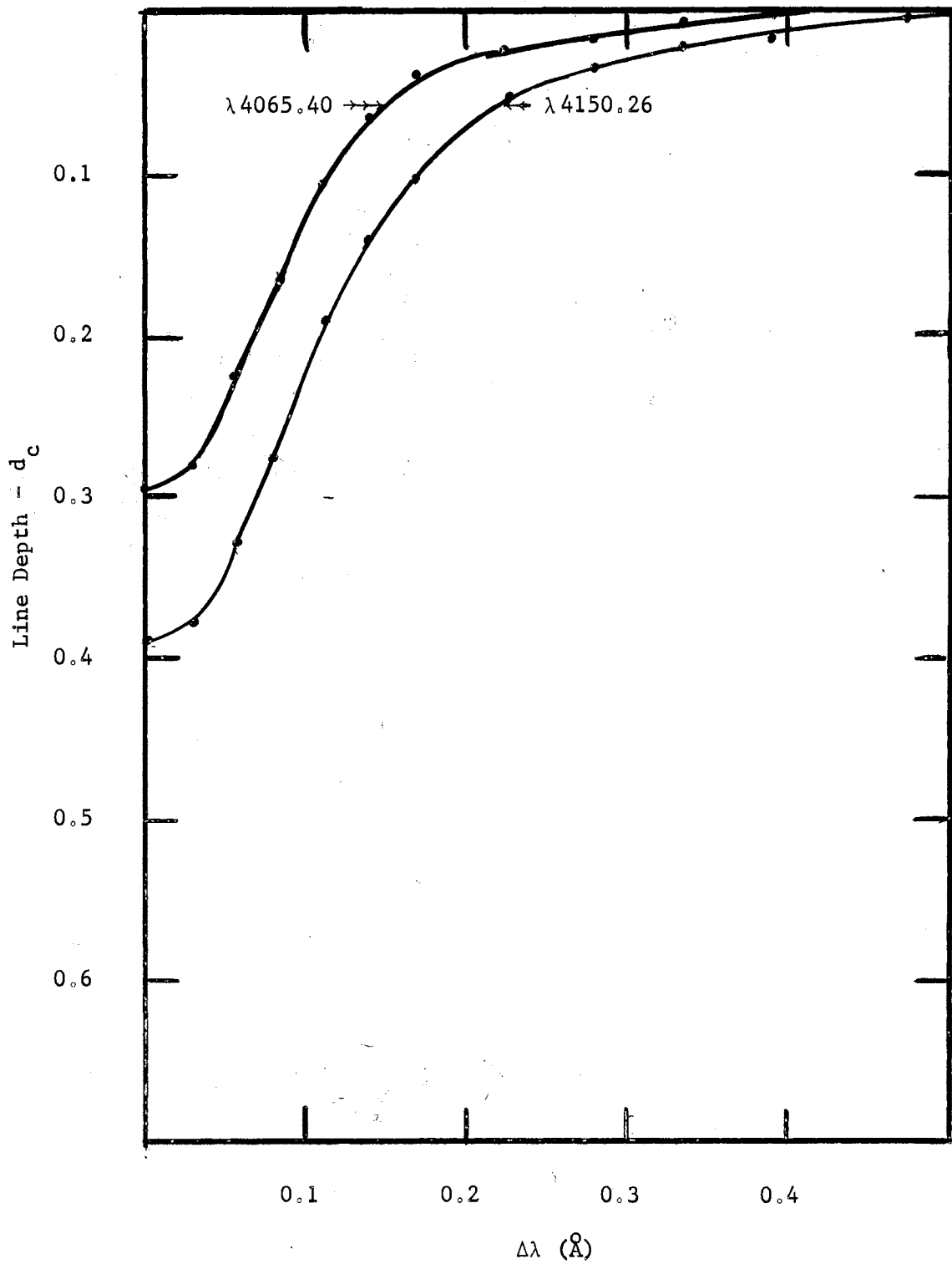


Figure 18. Observed Profiles of Two Null Lines of Singly Ionized Iron

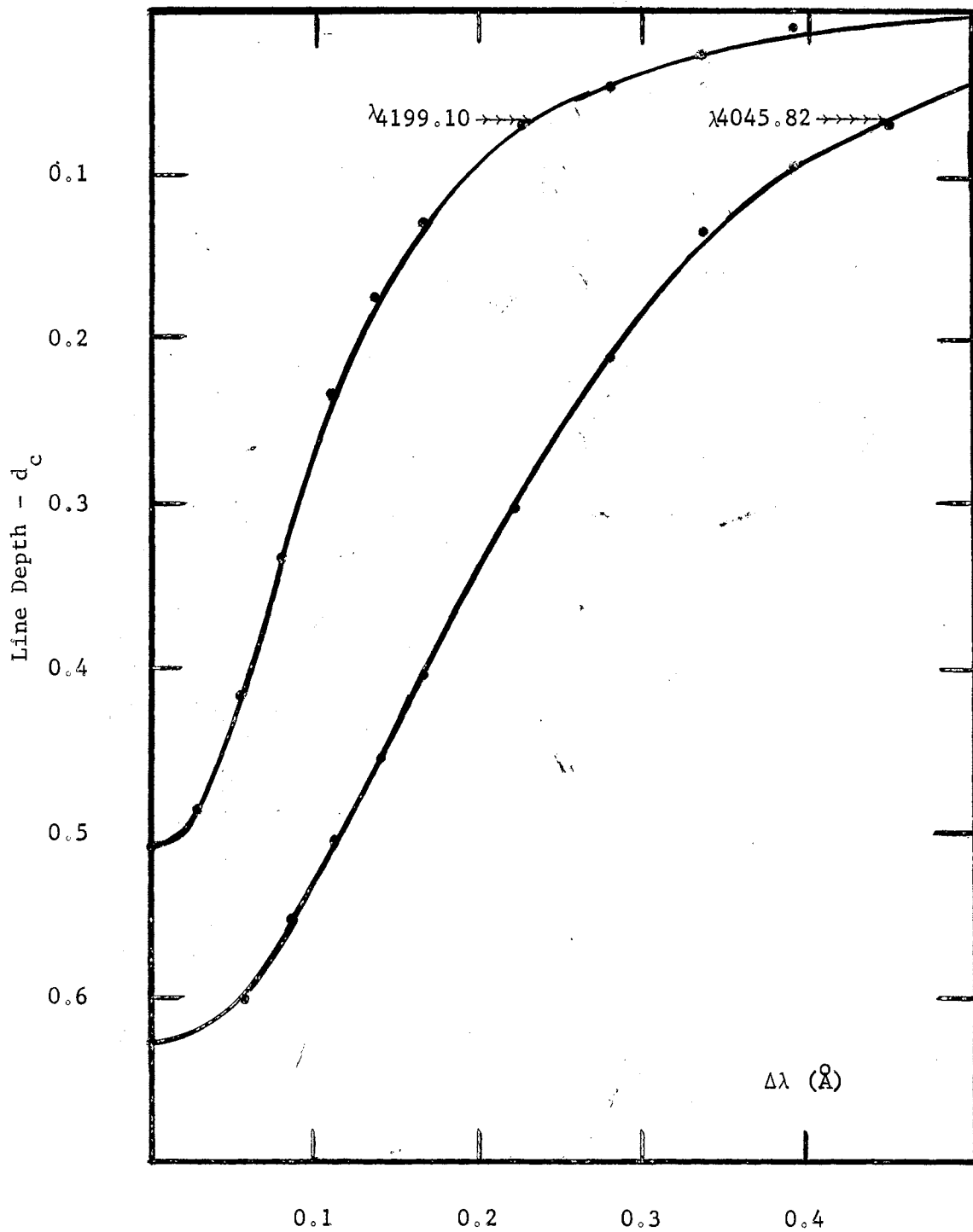


Figure 19. Observed Profiles of the Magnetically Sensitive Line  $\lambda 4045.82$  and the Line  $\lambda 4199.10$  of Singly Ionized Iron

### The Microturbulence Analysis

The turbulence broadening effects are commonly distinguished as being of two types, macroturbulence and microturbulence. Macroturbulence is defined as mass motions whose linear extent is large compared with the mean free path of a photon. On the other hand, for microturbulence the mass eddies have a linear extent small as compared with the mean free path of a photon. Turbulence influences both the equivalent width and the line profiles, but in a different manner. Microturbulence elements moving with different velocities absorb radiation from the continuous spectrum at different distances from the line center resulting in a broadening of the line profile and an increased equivalent width. The delaying of optical saturation then raises the flat portion of the curve of growth, as can be seen in Figure 20, for various microturbulent velocities. Whereas, macroturbulence and stellar rotation do not influence the equivalent width, since macroturbulence occurs after the line has been formed and simply rounds out the line profile.

For Beta Coronae Borealis, the most important sources of line broadening arise from Doppler broadening brought about by thermal phenomena and atmospheric microturbulence. A term  $\epsilon$ , whose value is the most probable velocity of the assumed Gaussian distribution within a small volume element along the line of sight, is included in the Doppler width term, or,

$$\Delta\lambda_o = \frac{\lambda}{c} \left( \frac{2kT}{m} + \epsilon^2 \right)^{1/2}$$

which represents the convolution of the thermal and microturbulence profiles. The term,  $2kT/m$  is the most probable velocity squared of the

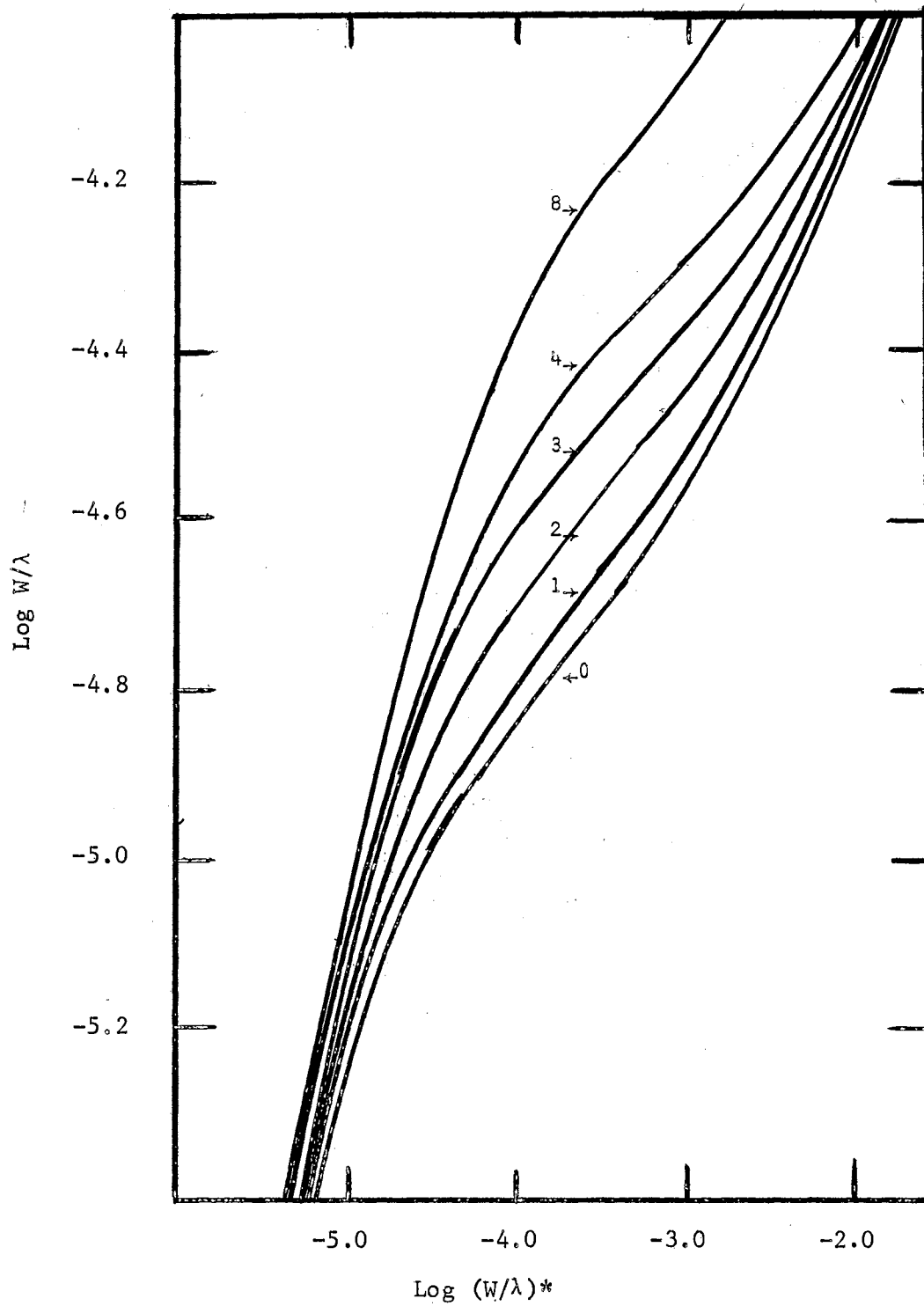


Figure 20. Theoretical Curve of Growth for Neutral Iron with the Labeled Microturbulent Velocities (km/sec)

gas atoms.

The existence of microturbulence can best be determined from the curve of growth. Microturbulence produces an effective Doppler broadening which tends to delay the onset of optical saturation and effects the transition region of the curve of growth. Huang and Struve (1960) discuss this effect in some detail in their reviews on atmospheric turbulence. On the other hand, if the scale of the turbulence is large (macroturbulence) the effect upon the equivalent width is negligible but the line profile will be altered as in stellar rotation. The sharpness of the absorption lines in Beta Coronae Borealis suggests that both the macroturbulence and stellar rotation are small.

From the analysis of the profile of a line, Huang and Struve in 1954 first developed a method for the separation of these two broadening mechanisms. Through a curve of half-half width correlation, a plot of the functional dependence of the half-width of a spectral line upon its equivalent width, they developed a procedure whereby the shift in the vertical and horizontal axis necessary to fit the empirical to the theoretical curve could be combined to derive a value for both large and small scale turbulent effects. The observed relation of the Huang-Struve method is displayed in Figure 21 but no theoretical calculations have been carried out here. Van den Heuvel (1963) and Elste (1967) have employed a similar curve to distinguish between macroturbulence and microturbulence. However, their approach is to calculate the theoretical relation using a model atmosphere, and so gives a more exact relationship between  $\log h/\lambda$  and  $\log W/\lambda$  than did Huang and Struve. This approach will be used here while using the model atmosphere furnished by Dr. John D. Evans of Kansas State University for a similar A-star,

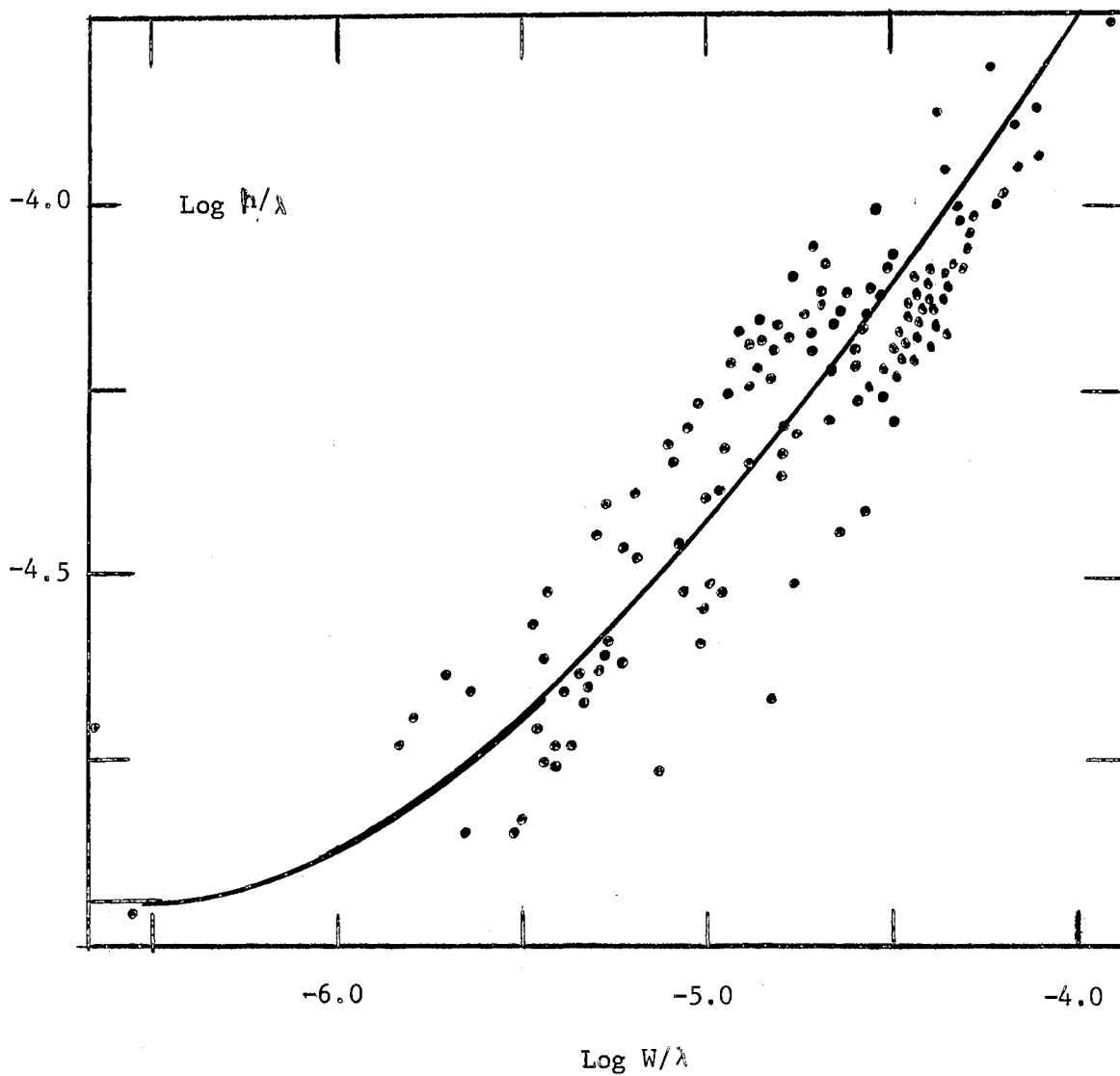


Figure 21. Observed Relation Between  $\text{Log } W/\lambda$  and  $\text{Log } h/\lambda$  for Beta Coronae Borealis

Gamma Equulei.

The absorption line intensities of seventeen lines of neutral iron were used for the curve of growth analysis. The line intensities for iron have been incorporated into Table IV, Chapter II, and the results of the computerized curve of growth analysis have been included in Table X. Likewise, the line intensities for chromium have been incorporated into Table III, Chapter II, and the results of the computerized curve of growth analysis have been included in Table X.

The  $f$ -values for neutral iron, as well as for the other elements of various ionization stages, were taken mainly from the compilation of Corliss and Bozeman (1962), Corliss and Warner (1964) and Corliss and Tech (1968). Since the  $f$ -values of Corliss and Tech have been shown to contain a systematic dependence upon the excitation potential (Wares, Wolnik, and Berthel 1970; Evans, Weems, and Schroeder 1970) an attempt was introduced to correct for this uncertainty by using the results of Evans, Weems, and Schroeder. For multiplets of Fe I falling within the wavelength region of 4200 angstroms, the  $f$ -values were lowered 0.5 dex (dex corresponds to log base 10) for those multiplets with an excitation potential greater than 2.2 electron volts. Multiplets with an excitation potential less than 2.2 electron volts were left unchanged. In addition to this correction suggested by Evans, Weems, and Schroeder (1970), an attempt was made to find numerous  $f$ -values for each transition using somewhat of a statistical approach to the correct  $f$ -value. Table IX shows a comparison of various log  $gf$  values for neutral iron transitions. The  $f$ -values can be experimentally obtained by various methods, each of which has some uncertainty. Some of the experimental methods for obtaining  $f$ -values include the following: (a) absorption



TABLE IX  
 COMPARISON OF VARIOUS LOF gf VALUES  
 FOR NEUTRAL IRON TRANSITIONS

$\lambda$	CB	CW	others	IC	Best
3767.19	-0.01		-0.07,+0.05		-0.01
3849.97	-0.43		-0.45,-0.46		-0.44
4045.82	+0.72		+0.69,+0.62,+0.59		+0.68
4065.40		-0.71		-0.69	-0.70
4071.74	+0.36		+0.43,+0.42,+0.34		+0.40
4137.00		+0.09		+0.15	+0.12
4143.42	+0.62			+0.59	+0.61
4143.87	-0.12		-0.08,-0.01,-0.16		-0.07
4150.26		-0.77		-0.64	-0.71
4153.91		+0.33		+0.34	+0.33
4157.79		+0.17		+0.16	+0.17
4187.04	+0.26	+0.14	+0.06	+0.21	+0.17
4187.80	+0.23	+0.13	+0.04	+0.21	+0.13
4202.03	-0.29		-0.18,-0.21	-0.31	-0.25
4210.35	-0.23	-0.13		-0.20	-0.19
4235.94	+0.33	+0.27	+0.36,+0.28	+0.29	+0.31
4238.82	+0.40	+0.37	+0.67	+0.42	+0.47
4250.12	+0.22	+0.23	+0.46,+0.12	+0.23	+0.25
4250.79	-0.38		-0.30,-0.22,-0.37	-0.24	-0.28
4271.16	+0.19	+0.29	+0.36,+0.23	+0.18	+0.25
4271.76	+0.16	+0.25	+0.21		+0.20
4282.41	-0.26	-0.18	-0.02	-0.17	-0.16

TABLE X  
ABUNDANCE RESULTS

Element	RMT	Wavelength	Chi (L)	Log gf	Log gfλ	Log C	Log (W/λ)*	Log W/λ	Wt.	Log N/N(H)
Cr II	26	4179.43	3.83	-1.09	-5.4689	1.9490	-2.3466	-4.2200	2	-4.2956
Cr II	31	4252.62	3.86	-1.02	-5.3913	2.0049	-2.9212	-4.4200	2	-4.9261
Cr II	31	4261.92	3.86	-1.21	-5.5804	1.8159	-2.6648	-4.3300	2	-4.4807
Cr II	31	4275.57	3.86	-1.33	-5.6990	1.6973	-3.0753	-4.4700	2	-4.7726
Fe I	42	4202.03	1.48	-0.25	-4.6265	2.0193	-2.7825	-4.4400	2	-4.8018
Fe I	42	4250.79	1.56	-0.28	-4.6515	1.9347	-2.5179	-4.3500	2	-4.4526
Fe I	43	4071.74	1.61	+0.40	-3.9902	2.5588	-2.6307	-4.3900	2	-5.1895
Fe I	43	4143.87	1.56	-0.07	-4.4526	2.1336	-2.4632	-4.3300	2	-4.6839
Fe I	71	4282.41	2.18	-0.16	-4.5283	1.5977	-3.0063	-4.4900	2	-4.6040
Fe I	152	4187.04	2.45	+0.17	-4.2081	1.7185	-2.4062	-4.2800	2	-4.1247
Fe I	152	4210.35	2.48	-0.19	-4.5657	1.3388	-2.8150	-4.4300	2	-4.1537
Fe I	152	4235.94	2.42	+0.31	-4.0631	1.8857	-2.6152	-4.3600	2	-4.5009
Fe I	152	4250.12	2.47	+0.25	-4.1216	1.7902	-2.9078	-4.4600	2	-4.6980
Fe I	152	4271.16	2.45	+0.25	-4.1195	1.8071	-2.7852	-4.4200	2	-4.5923
Fe I	523	4143.42	3.05	+0.61	-3.7726	1.7140	-2.8150	-4.4300	2	-4.5290
Fe I	693	4238.82	3.40	+0.47	-3.9028	1.3292	-2.4842	-4.3100	2	-3.8116
Fe I	695	4150.26	3.43	-0.71	-5.0919	0.1182	-3.4387	-4.6000	2	-3.5569
Fe I	695	4153.91	3.40	+0.33	-4.0515	1.1804	-2.2578	-4.2200	2	-3.4382
Fe I	695	4157.79	3.42	+0.17	-4.2111	1.0063	-2.8762	-4.4500	2	-3.8825
Fe I	698	4065.40	3.43	-0.70	-5.0909	0.1192	-4.2113	-4.8000	2	-4.3305
Fe I	726	4137.00	3.41	+0.12	-4.9614	0.9614	-2.4062	-4.2800	2	-3.3675

tube, (b) arc, (c) flame, (d) Hook method, (e) pressure broadening, (f) magneto rotation, and (g) lifetimes. Theoretical methods include the following: (a) self consistent field, (b) coulomb approximation, (c) other quantum mechanical calculations, (d) quantum mechanical calculations for forbidden lines, (e) estimation from sum rules, and (f) interpolation within isoelectronic sequences, spectral series and homologous atoms. As past studies have shown, experimental values appear to be much more accurate than theoretical calculations, so in this study the experimental values are used.

The curves of growth for iron are shown in Figure 22 and Figure 23. All curves of growth have been computed for the center of the star's disk. In Figure 23 the lower curve represents the curve of growth for the region of 4200 angstroms broadened only by random thermal motion of atoms in the stellar atmosphere. The fact that the data lie on both sides of this curve indicated that the macroturbulent velocity of this region is small if it exists at all. The upper curve, which is labeled with a 1.5 kilometer per second microturbulent velocity, seems to represent the average value over this wavelength range. Figures 24 and Figure 25 display the theoretical and empirical curves of growth for singly ionized chromium.

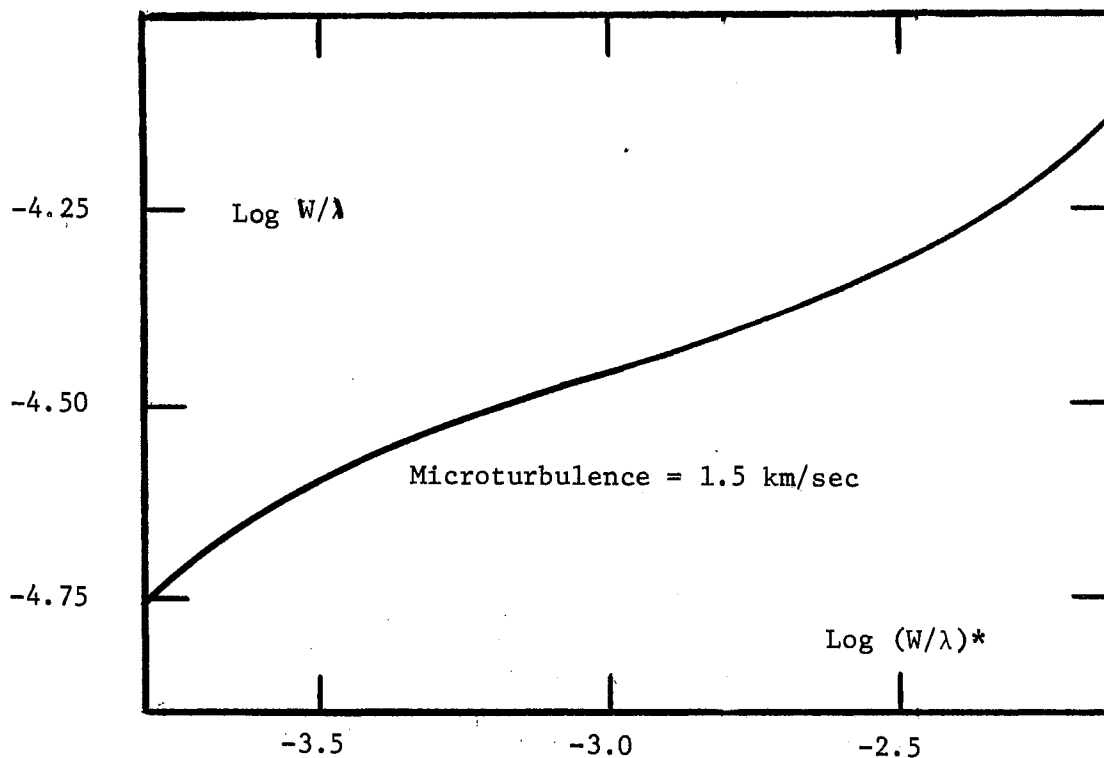


Figure 22. Theoretical Curve of Growth for Fe I

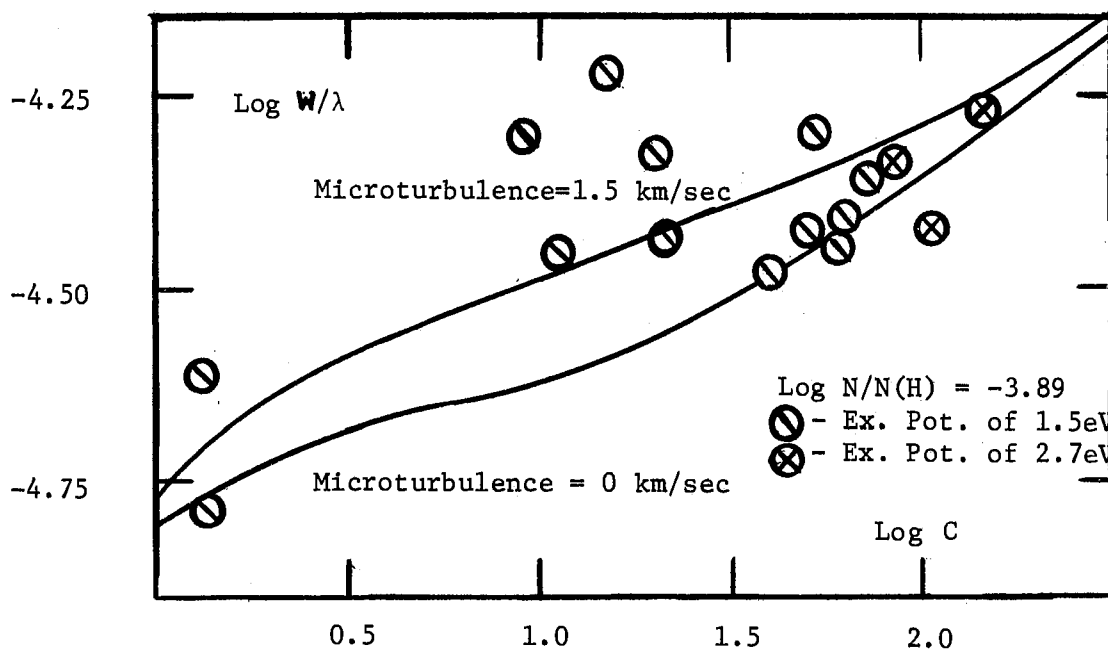


Figure 23. Empirical Curve of Growth for Fe I

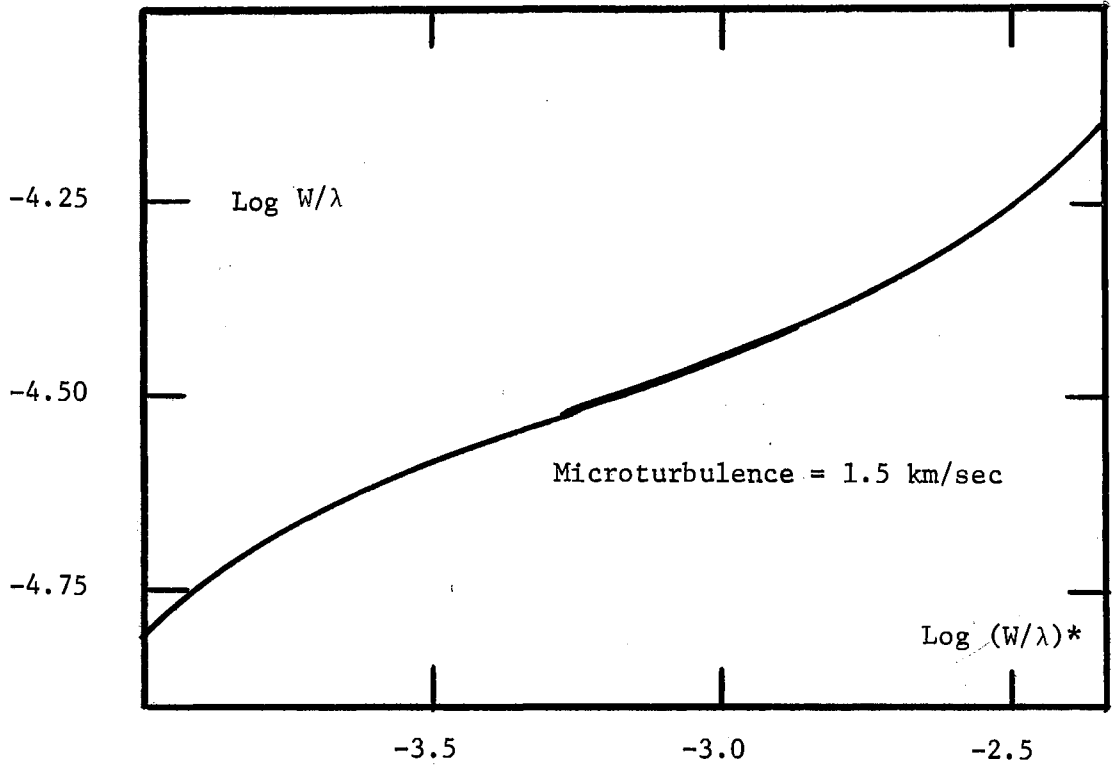


Figure 24. Theoretical Curve of Growth for Cr II

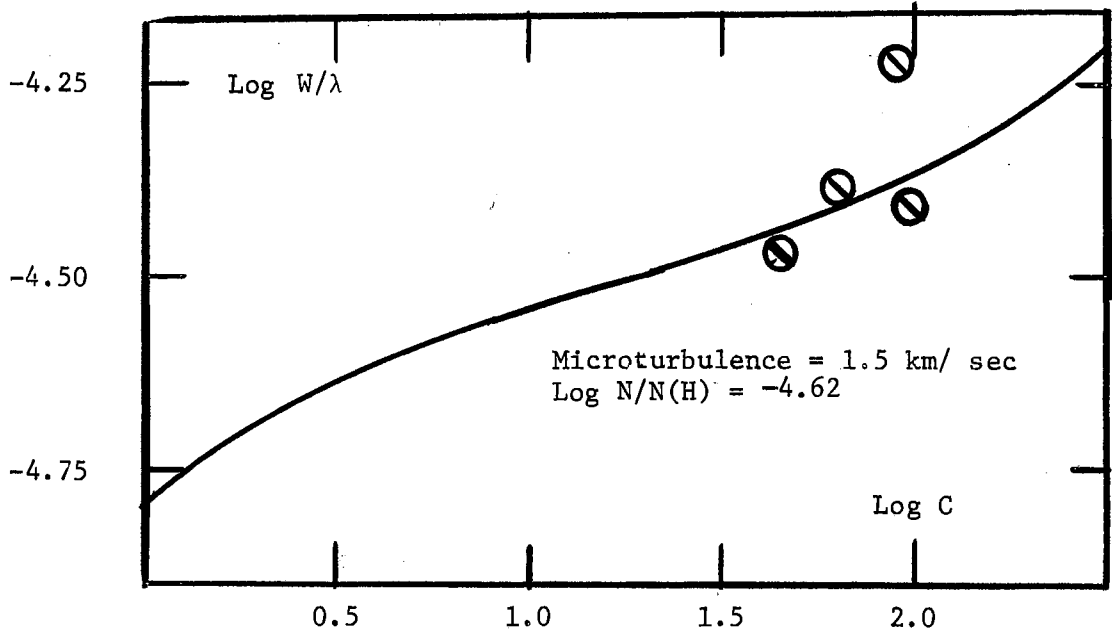


Figure 25. Empirical Curve of Growth for Cr II

## CHAPTER V

### SUMMARY AND CONCLUSIONS

#### The Turbulence Model

The presence of small scale mass motions, microturbulence, in the atmosphere of Beta Coronae Borealis was investigated from an analysis of the neutral iron lines using a model atmosphere of a similar A-star, Gamma Equulei. The computer programs for the model atmosphere and the curves of growth were provided by Dr. John Evans of Kansas State University. Using the Oklahoma State University computer facilities, both the theoretical and empirical curves of growth were computed for the model atmosphere selected for Beta Coronae Borealis. In order to achieve a reasonable fit between the empirical and calculated curve, it was necessary to include a small microturbulent velocity of 1.5 kilometer per second. This value of microturbulence is somewhat smaller than the 4 kilometers per second value reported by Hack (1958).

Overall, the line profiles were sharp instead of wide and boxy-bottomed, which suggests that the large scale mass motions, macroturbulence, are very small if they even exist in the atmosphere of Beta Coronae Borealis. In this study the actual macroturbulent velocity has not been calculated. From the correlation existing between the half-width of a line and its equivalent width, an assessment of the amount of macroturbulent motion in the stellar atmosphere could be calculated.

## The Abundances

The preliminary abundances of neutral iron and singly ionized chromium found to exist in the atmosphere of Beta Coronae Borealis were determined by using the Van den Heuvel (1963) and Elste (1967) method, whereby a model atmosphere is used to calculate the theoretical relation for the curve of growth. Absorption line selection was based upon the availability and the quality of observational data of this star. A few absorption lines were discarded for the abundance analysis due to their respective  $gf$ -values not being available. The abundance for each line was computed using a theoretical curve of growth based upon the analysis of the neutral iron lines for the microturbulence determination.

For singly ionized chromium, as well as for neutral iron, it appeared that the theoretical and empirical curves of growth agreed more correctly for this 1.5 kilometer per second microturbulent velocity than for any other value of microturbulence.

### Neutral Iron

Using a 1.5 kilometer per second microturbulent velocity the abundance of neutral iron relative to hydrogen in the atmosphere of Beta Coronae Borealis is

$$\text{Log } \frac{N(\text{Fe I})}{N(\text{H})} = -3.89$$

which is about 5.1 times more abundant than it is in the solar photosphere. The most recent adopted abundances in the solar photosphere have been compiled by G. L. Withbroe (1971). As is shown in Table XI, our relative abundance is in very good agreement with the value determined by Hack (1958), who used a microturbulent velocity of 4 kilometers

per second. The neutral iron excitation potential for the considered atomic transitions ranged from 1.48 electron volts to 3.43 electron volts.

### Singly Ionized Chromium

Using a 1.5 kilometer per second microturbulent velocity the abundance of singly ionized chromium relative to hydrogen in the atmosphere of Beta Coronae Borealis is

$$\text{Log } \frac{N(\text{Cr II})}{N(\text{H})} = -4.62$$

which is about 47 times more abundant than it is in the solar photosphere, according to the most recent adopted compilation (Withbroe 1971). As is shown in Table XI, this relative abundance is 5 times greater than the value obtained by Hack (1958) who used a microturbulent velocity of 4 kilometers per second. The discrepancy in the two values obtained can probably be accounted for in the respective gf-values used. Many compilations of transition probabilities have systematic errors resulting from the negligence to observe the dependence of the gf-value on the excitation potential of the upper level. Bridges (1970) has found that Fe I gf-values were in good agreement when measured by shock-tube absorption, emission in wall stabilized arcs, and lifetime measurements. A more refined analysis concerning the selection of the gf-values might yield more definitive abundance results.

### Possible Future Research Projects

As well as the actual determination of the macroturbulent motion in the atmosphere of Beta Coronae Borealis, future research could include a detailed abundance analysis of all the identified elements in the atmosphere of Beta Coronae Borealis for which adequate numbers of lines and



TABLE XI

## ABUNDANCE RESULT COMPARISON

Element and Ionization	Adopted Solar Abundance	Beta Coronae Borealis				
		Opitz			Hack	
	Withbroe (1971)	$\text{Log } \frac{N}{N(H)}$	$\text{Log } \frac{N^*}{N_{\odot}}$	$\frac{N^*}{N_{\odot}}$	$\text{Log } \frac{N^*}{N_{\odot}}$	$\frac{N^*}{N_{\odot}}$
Fe I	-4.60	-3.89	+0.71	5.1	+0.70	5.0
Cr II	-6.30	-4.62	+1.68	47.8	+0.94	8.7

gf-values are available.

Also, the surface magnetic field strength could be determined using the equivalent widths of the null lines as well as the magnetically sensitive lines (Shore and Adelman 1974).

SELECTED BIBLIOGRAPHY

- Abt, H. A. and Golson, J. C. 1962, Ap. J., 136, 363.
- Adelman, S. J. 1973, Ap. J., 183, 95.
- \_\_\_\_\_. 1974, private communication.
- Adelman, S. J., and Shore, S. N. 1973, Ap. J., 183, 121.
- Adelman, S. J., Shore, S., and Tiernan, M. 1973, Ap. J., 186, 605.
- Allen, C. W. 1955, Astrophysical Quantities (London: Athlone Press).
- Aller, L. H. 1963, Astrophysics (2nd. ed.; New York: The Ronald Press Company).
- Aller, L. H., Elste, G. and Jugaku, J. 1957, Ap. J. Suppl. 3, 1.
- Babcock, M. W. 1947, Ap. J., 105, 105.
- \_\_\_\_\_. 1958, Ap. J. Suppl. 3, 141.
- \_\_\_\_\_. 1963, Annual Review of Astronomy and Astrophysics (Palo Alto: Annual Review, Inc.), Vol. 1, p. 41.
- Burbidge, G. R., and Burbidge, E. M. 1955, Ap. J. Suppl. 1, 431.
- Corliss, C. H. 1967, NBS Monograph No. 32 (Washington, D.C.: Department of Commerce).
- Corliss, C. H. and Bozeman, W. R. 1962, NBS Monograph No. 53 (Washington, D.C.: Department of Commerce).
- Corliss, C. H. and Tech, J. L. 1968, NBS Monograph No. 108, (Washington, D.C.: Department of Commerce).
- Corliss, C. H. and Warner, B. 1964, Ap. J. Suppl. 8, 395.
- Fred, M. and Tomkins, F. S. 1957, J. Opt. Soc. Am., 47, 1076.
- Elste, G. 1967, Ap. J., 148, 857.
- Evans, J. C. 1966, Ph.D. Thesis, University of Michigan, unpublished.

- \_\_\_\_\_. 1974, private communication.
- Evans, J. C. and Schroeder, L. W. 1969, Bull. Am. Astron. Soc., Vol. 1, No. 1, p. 341.
- Evans, J. C., Weems, M. L. B., and Schroeder, L. W. 1970, Bull. Am. Astron. Soc., Vol. 3, No. 1, pt. 1, p. 10.
- Glad, S. 1956, Ark. Fys. (Stockholm), 10, 291.
- Glennon, B. M. and Wiese, W. L. 1962, NBS Monograph No. 50 (Washington, D.C.: Department of Commerce).
- Gray, D. F. and Evans, J. C. 1973, J. Roy. Astr. Soc. Can., 67, 241.
- Gruber, J. D. 1972, Ed.D. Thesis, Oklahoma State University, unpublished.
- Haagland, J. 1957, JENER REPORT No. 51, Kjeller, Norway Joint Establishment for Nuclear Energy Research.
- Hack, M. 1958, Mem. S.A.I., 29, 263.
- \_\_\_\_\_. 1961, Mem. S.A.I., 31, 280.
- Hardorp, J. and Shore, S. N. 1971, Pub. A.S.P., 83, 605.
- Harrison, G. R. 1969, The Massachusetts Institute of Technology Wavelength Tables. Cambridge, Massachusetts and London, England. The M.I.T. Press.
- Heuvel, E. P. J. van den. 1963, B.A.N., 17, 148.
- Hiltner, W. A. 1945, Ap. J., 102, 438.
- Huang, S. S. and Struve, O. 1954, Ap. J., 116, 410.
- \_\_\_\_\_. 1960, Stellar Atmospheres, ed. J. L. Greenstein (Chicago: University of Chicago Press) p. 321.
- Humphreys, C. J. 1939, J. Res. N.B.S., 22, 19.
- Jordan, T. M. 1974, M.S. Thesis, Oklahoma State University, unpublished.
- Jugaku, J., and Sargent, W. L. W. 1968, Ap. J., 151, 159.
- Kiess, C. C. 1951, J. Res. N.B.S., 47, 385.
- \_\_\_\_\_. 1953, ibid., 51, 247.
- \_\_\_\_\_. 1958, ibid., 60, 375.
- Meggers, W. F. 1957, Spectrochimica Acta, 10, 195.

- Miles, B. M. and Wiese, W. L. 1970, N.B.S. Special Publication No. 320  
(Washington, D.C.: Department of Commerce).
- Minnaert, M. S. and Slob, C. 1931, Proc. Amsterdam Acad., 34, pt. 1,  
542.
- Moore, C. E. 1959, A Multiplet Table of Astrophysical Interest (revised  
edition) Contr. Princeton U. Obs., No. 20, 1945.
- Neubauer, F. J. 1944, Ap. J., 99, 134.
- Peebles, H. O. 1964, Ph.D. Thesis, Oklahoma State University, unpub-  
lished.
- Preston, G. W. 1971, Ap. J., 164, 309.
- Preston, G. W. and Pyper, D. M. 1965, Ap. J., 142, 983.
- Regemorten, H. van. 1965, Annual Review of Astronomy and Astrophysics  
(Palo Alto: Annual Reviews, Inc.), Vol. 3, p. 71.
- Sargent, L. W. and Searle, L. 1962, Ap. J., 136, 408.
- Schroeder, L. W. 1958, Ph.D. Thesis, Indiana University, unpublished.
- Shenstone, A. G. 1970, J. Res. N.B.S., 74A, 801.
- Shore, S. N. and Adelman, S. J. 1974, Ap. J., 191, 165.
- Shore, S. N. and Hardorp, J. 1974, in preparation.
- Strömberg, B. 1940, Pub. Copenhagen Obs., Vol. 1, 127.
- Struve, O. and Elvey, C. T. 1934, Ap. J., 79, 409.
- Thackeray, A. 1936, Ap. J., 84, 433.
- Unsold, A. O. J. 1969, Science, 163, 1015.
- Wares, G. W., Wolnick, S. S. and Berthel, R. O. 1970, Ap. J., 162, 1037.
- Weems, M. L. B. 1972, Ph.D. Thesis, Oklahoma State University, unpub-  
lished.
- Wiese, W. L., Smith, M. W. and Miles, B. M. 1969, NSRDS-NBS No. 22  
(Washington, D.C.: U.S. Government Printing Office), Vol. 2, p. 1.
- Wiese, W. L. 1970, Nuc. Inst. and Meth., 90, 25.
- Withbroe, G. L. 1971, NBS Spec. Publ. 353, 127.
- Wolff, S. C. and Bonsack, W. K. 1972, Ap. J., 176, 425.
- Wolff, S. C. and Morrison, N. D. 1971, Pub. A.S.P., 83, 609.

VITA  $\gamma$

Ronald Marcus Opitz

Candidate for the Degree of

Master of Science

**Thesis:** A PRELIMINARY ABUNDANCE ANALYSIS AND MICROTURBULENCE  
DETERMINATION FOR THE PECULIAR A-STAR BETA CORONAE  
BOREALIS

**Major Field:** Physics

**Biographical:**

**Personal Data:** Born in Fort Cobb, Oklahoma, January 5, 1949, the son of Rudy M. and Dorothy J. Opitz.

**Education:** Attended grade school in Fort Cobb and Oney, Oklahoma; graduated from Asher High School, Asher, Oklahoma in May 1967; received the Bachelor of Science degree from East Central Oklahoma State University, Ada, in May, 1971 with majors in Physics and Mathematics; received an Electronics Technology degree from the Cleveland Institute of Electronics in December, 1973; completed requirements for the Master of Science degree in December, 1974.

**Professional Experience:** Undergraduate Teaching Assistant, East Central State College, Department of Physics, 1969-70; Chief of Security, Nike Hercules Missile Base, U.S. Army, 1972-73; Graduate Teaching Assistant, Oklahoma State University, Department of Physics, 1971 and 1973-74.